



1 **Assessment of Arctic and Antarctic Sea Ice Predictability in CMIP5 Decadal Hindcasts**

2

3 Chao-Yuan Yang¹, Jiping Liu¹, Yongyun Hu², Radley M. Horton³, Liqi Chen⁴, Xiao Cheng⁵

4

5 ¹Department of Atmospheric and Environmental Sciences, University at Albany, State University
6 of New York, Albany, NY, USA

7 ²Department of Atmospheric and Oceanic Sciences, School of Physics, Peking University,
8 Beijing, China

9 ³Columbia University Center for Climate Systems Research and NASA Goddard Institute for
10 Space Studies, New York, NY, USA

11 ⁴Key Laboratory of Global Change and Marine-Atmospheric Chemistry, Third Institute of
12 Oceanography, SOA, Xiamen, China

13 ⁵College of Global Change and Earth System Science, Beijing Normal University, Beijing, China

14

15

16

17

18 Corresponding author:

19 Chao-Yuan Yang

20 Department of Atmospheric and Environmental Sciences

21 University at Albany, State University of New York

22 Albany, NY, 12222 USA

23 Email: cyang4@albany.edu



24 **Abstract**

25 This paper examines the ability of coupled global climate models to predict decadal
26 variability of Arctic and Antarctic sea ice. We analyze decadal hindcasts/predictions of 11
27 CMIP5 models. Decadal hindcasts exhibit a large multi-model spread in the simulated sea ice
28 extent, with some models deviating significantly from the observations. For the models having
29 large biases and using full-field initialization, the predicted sea ice extent quickly drifts away
30 from the initial constraint, deteriorating the decadal predictive skill. The anomaly correlation
31 analysis between the decadal hindcast and observed sea ice suggests that in the Arctic, for most
32 models, the areas showing significant predictive skill become broader associated with increasing
33 lead times. This area expansion is largely because nearly all the models are capable of predicting
34 the observed decreasing Arctic sea ice cover. Sea ice extent in the north Pacific has better
35 predictive skill than that in the north Atlantic (particularly at a lead-time of 3-7 years), but there
36 is a re-emerging predictive skill in the north Atlantic at a lead-time of 6-8 years. In contrast to
37 the Arctic, Antarctic sea ice decadal hindcasts do not show broad predictive skill at any time
38 scales, and there is no obvious improvement linking the areal extent of significant predictive skill
39 to lead-time increase. This might be because nearly all the models predict a retreating Antarctic
40 sea ice cover, opposite to the observations. For the Arctic, the predictive skill of the MMEE
41 outperforms most models and the persistence prediction at longer time scales, which is not the
42 case for the Antarctic.

43



44 **1. Introduction**

45 Decadal climate prediction is a new and rapidly evolving research area driven by societal
46 demand for climate information to inform climate adaptation strategies (e.g., Meehl et al., 2009,
47 2013; Vera et al., 2010). As a boundary between the ocean and atmosphere, sea ice plays an
48 important role in the climate system and acts as an important indicator of climate change through
49 dynamic and thermodynamic processes and various feedbacks (i.e., albedo, insulation and
50 buoyancy). Thus, sea ice simulation and prediction is one of the most challenging and important
51 issues in decadal climate prediction, i.e., Meehl et al. (2009) emphasized the importance of sea
52 ice treatment in climate models as large uncertainties remain for decadal climate prediction.

53 In the past few decades, Arctic sea ice has been declining (e.g., Serreze et al., 2007; Arctic
54 Report Card, 2015). Trends in Arctic sea ice extent are negative for all months (e.g., Comiso,
55 2008, 2012; Cavalieri and Parkinson, 2012) largely due to thinning and loss of the perennial sea
56 ice cover (Kwok et al., 2009), but are largest at the end of the summer melt season. September
57 Arctic sea ice extent has declined by $0.87 \times 10^6 \text{ km}^2$ for the period 1979-2014, with a pronounced
58 decreasing trend of sea ice concentrations in the arc extending from the Beaufort Sea to the
59 Barents Sea (> 95% significance, Fig. 1a). The possibility of an ice-free Arctic in the coming
60 decades (Stroeve et al., 2007, 2012; Boé et al., 2009; Wang and Overland, 2009, 2012; Zhang,
61 2010; Massonnet et al., 2012; Liu et al., 2013) would have profound impacts on Arctic maritime
62 activities (e.g., opening of shorter shipping routes) and ecosystems (e.g., changing solar radiation
63 in the upper ocean and influencing primary productivity), and extreme weather and climate in
64 mid- and high-latitudes (e.g., Liu et al., 2012; Francis and Vavrus, 2012; Smith and Stephenson,
65 2013; WWRP/PPP, 2013; Stroeve et al., 2014).



66 By contrast, Antarctic sea ice has been expanding (e.g., Liu et al., 2004; Turner et al., 2009;
67 Comiso et al., 2011; Parkinson and Cavalieri, 2012). Trends in Antarctic sea ice extent are
68 positive for all months. Unlike the almost uniform Arctic sea ice decreases, the trends in
69 Antarctic sea ice concentrations show strong regional variations, although the NASA's Ice,
70 Cloud, and land Elevation Satellite showed that Antarctic sea ice thickness has a small negative
71 trend during 2003-2008 (Kurtz and Markus, 2012). September Antarctic sea ice extent has
72 increased by 0.24×10^6 km² per decade during 1979-2014, with a pronounced positive trend of
73 sea ice concentrations in the Ross Sea partially offset by a negative trend in the Bellingshausen
74 and Weddell Seas (Fig. 1b). The limited understanding of some of the mechanisms responsible
75 for the observed decrease (increase) in Arctic (Antarctic) sea ice makes sea ice prediction
76 challenging (e.g., Kattsov et al., 2010; Richter-Menge et al., 2012; Bindoff et al., 2013; Goosse
77 et al., 2015).

78 Most sea ice predictability studies have focused on the Arctic and the
79 seasonal-to-interannual time scale. An outlook of September Arctic sea ice extent has been
80 solicited from research community since 2008. Stroeve et al. (2014) showed that the median July
81 (the same was true for June and August) prediction value for September sea ice cover was off by
82 a large margin in 2009, 2012 (record low), and 2013. Koenigk and Mikolajewicz (2009)
83 suggested sea ice cover has low predictability in the central Arctic but some predictability at sea
84 ice edge zones in the MPI ECHAM5-OM climate model. Holland et al. (2011) showed potential
85 predictability of sea ice cover with a few months lead-time in the NCAR Community Climate
86 System Model version 3 (CCSM3). They also suggested that the persistence of sea ice thickness
87 anomalies is much higher than that of sea ice extent anomalies, which might point to a pathway
88 towards greater predictability as models improve their simulation of sea ice thickness.



89 Predictability of sea ice cover with e-folding time scales of 2-5 months has been identified in
90 several climate models (Day et al., 2014a). A few modeling studies also showed continuous
91 predictability of sea ice cover for 1-2 years, and intermittent predictability for 2-4 years
92 (Blanchard-Wrigglesworth et al., 2011b; Day et al., 2015; Tietsche et al., 2013, 2014; Guemas et
93 al., 2014). In contrast to the Arctic, there are limited efforts on examining predictability of
94 Antarctic sea ice. Using the NCAR CCSM3 model, Holland et al. (2013) showed initial-value
95 predictability of sea ice for a few months in the edge around Antarctica.

96 To date, relatively little attention has been paid to assessing prediction skill of sea ice at
97 decadal timescales for the Arctic and Antarctic in current-day climate models. Decadal sea ice
98 prediction entails a combination of initial value and climate forcing issues. At decadal timescales,
99 internal climate variability affects sea ice (i.e., some aspects of climate internal variability may
100 be predictable, Collins and Allen, 2002; Smith et al., 2007; Keenlyside et al., 2008; Meehl et al.,
101 2009; Pohlmann et al., 2009; Mochizuki et al., 2012), as does prescribed external scenarios (e.g.,
102 greenhouse gases and other radiatively important agents). Blanchard-Wrigglesworth et al. (2011b)
103 suggested that predictability of Arctic sea ice beyond 3 years is largely influenced by climate
104 forcing rather than initial values. The growing dominance of climate forcings is likely to
105 introduce some potential predictability since it accounts for increasingly large portions of sea ice
106 change from present conditions (e.g., National Research Council, 2012). Guemas et al. (2014)
107 also underlined that predicting future change of Arctic sea ice on decadal timescales is
108 challenging due to initialization problems (i.e., the initial shocks due to sparse observations,
109 limitations of reanalysis data, and ensemble generation methods).

110 The recent Coupled Model Intercomparison Project Phase 5 (CMIP5) has implemented an
111 experiment to simulate and predict decadal climate variability (Meehl et al., 2009; Taylor et al.,



112 2012) in support of the Intergovernmental Panel in Climate Change Fifth Assessment Report.
113 The validation of decadal hindcasts is an important step for improving decadal predictions, since
114 it can elucidate issues in initialization methods and model responses to natural variability and
115 climate forcings. In this study, we examine the capability of CMIP5 decadal hindcasts to
116 simulate the mean and decadal variability of Arctic and Antarctic sea ice extent.

117 **2. Models and data**

118 Eleven CMIP5 models are used to evaluate the decadal hindcast/prediction of sea ice in both
119 the Arctic and Antarctic. These eleven models provide a set of 10-year long hindcast simulations,
120 which was initialized every five-years from 1981 to 2006. The purpose of initialization is to start
121 coupled global climate models close to the most realistic possible sea ice state. In general, the
122 initialization for the CMIP5 decadal hindcast/prediction can be divided into two approaches, full
123 initialization and anomaly initialization. For the full initialization approach, the initial model
124 state is replaced by the best available estimate of the observed sea ice state (i.e., satellite
125 observation and ocean analysis). This efficiently reduces the initial error due to the systematic
126 bias in the presence of model deficiencies. However, as the model is integrated for the decadal
127 hindcast/prediction, the simulation tends to drift away from the best-estimated sea ice state no
128 matter how small the initial error is. The anomaly initialization approach partly addresses this
129 problem by assimilating observed sea ice anomalies on the modeled sea ice state with focus on
130 predicting future sea ice anomalies.

131 Table 1 provides a summary of the initialization approaches and data source of the initial sea
132 ice state for each individual model. More detailed information about the set-up of the decadal
133 experiment can be found in Meehl et al. (2009) and Taylor et al. (2012). For each individual
134 model, all ensemble members of the 10-year long hindcast/prediction that are archived at



135 http://cmip-pcmdi.llnl.gov/cmip5/data_portal.html are used (see Table 1 for more information).
136 Each ensemble member was generated by slightly different initial conditions. Here we focus on
137 September Arctic (seasonal minimum) and Antarctic (seasonal maximum) sea ice. The reasons
138 that we focus on September Antarctic sea ice, rather than the month of seasonal minimum like
139 the Arctic are 1) sea ice in the Antarctic largely melts away (confined to the coastal Antarctica)
140 during the seasonal minimum (i.e. February or March), and 2) September sea ice extent has a
141 significant increasing trend.

142 Satellite-derived sea ice extent and concentration in the Arctic and Antarctic are used to
143 evaluate the CMIP5 decadal hindcast. They are obtained from the National Snow and Ice Data
144 Center, which are derived from the Nimbus-7 Scanning Multichannel Microwave Radiometer
145 (SSMR), and DMSP Special Sensor Microwave/Imager (SSM/I), and Special Sensor Microwave
146 Imager and Sounder (SSMIS) sensors (Comiso 2000; Fetterer et al., 2002, 2010). Because the
147 observation and models have different horizontal resolution (see details in Table 1), before
148 performing the assessment we interpolate all the data (satellite observation and model
149 simulations) to horizontal resolution of 1 degree. The multi-model ensemble mean (MMEE) is
150 calculated based on the equally weighted average of 69 total ensemble members (Table 1).

151 **3. Prediction skill of CMIP5 decadal hindcasts**

152 **3.1 Arctic sea ice**

153 We evaluate the model simulation and prediction skill by comparing sea ice extent between
154 each individual model and satellite observations. Figure 2 shows the time series of September
155 Arctic sea ice extent from the simulation of the 10-year hindcast for each model and observation
156 from 1981 to 2015. It is immediately apparent that the models exhibit very different magnitudes
157 of September sea ice extent. CanCM4, CFSv2, GEOS-5 and GFDL-CM2.1 simulate a smaller



158 ice extent compared to the observation during the entire period; CFSv2 has the least sea ice cover
159 of any of the models. By contrast, BCC-CSM1.1, CCSM4, FGOALS-g2 and MIROC5 simulate
160 a larger ice extent. The simulated ice extent of HadCM3, IPSL-CM5A-LR and MPI-ESM-MR
161 are comparable to the observations, but they cannot reproduce the anomalously low sea ice cover
162 since 2007 (i.e., record lows in 2007 and 2012). We note that the models that are initialized with
163 values close to various estimates of sea ice state (direct and indirect full-field initialization, see
164 Table 1), drift towards their modeled sea ice state within a few year integrations, particularly
165 BCC-CSM1.1, CanCM4, CCSM4, CFSv2 and FGOALS-g2. Hence improved initializations do
166 not necessarily mitigate drift, although they significantly reduce the model bias at the initial step.
167 By contrast, the models that are initialized with various estimates of sea ice anomaly (direct and
168 indirect anomaly initialization) tend to have smaller drift problems during the integration.

169 To quantify the skill of each individual model and MMEE in predicting the evolution of sea
170 ice, we calculate the anomaly correlation coefficient (ACC) between the predicted and observed
171 September sea ice concentration anomaly in each grid box as follows.

$$ACC = \frac{\sum_{i=1}^n [P(i, t) - \bar{P}(t)] \cdot [O(i, t) - \bar{O}(t)]}{\sqrt{\sum_{i=1}^n [P(i, t) - \bar{P}(t)]^2 \cdot \sum_{i=1}^n [O(i, t) - \bar{O}(t)]^2}}$$

172 where P is the predicted sea ice concentration and $\bar{P}(t)$ is calculated as $\bar{P}(t) = \sum_{i=1}^n P(i, t)$; O is
173 the observed sea ice concentration and $\bar{O}(t)$ is calculated as $\bar{O}(t) = \sum_{i=1}^n O(i, t)$. i is the start
174 year and t is the lead year. Here the ACCs of the ensemble mean of each individual model and
175 MMEE for lead-times of 1, 3-5 and 6-8 years are discussed. For example, for the lead-time of
176 3-5 years, the data for the 1981 initialization is the average value of 1983-1985, the data for the
177 1986 initialization is the average value of 1988-1990, and so on. This means the adjacent data



178 points in the time-series have a time interval of 5-years, and this time-series is compared to the
179 average of the same three years in the observations.

180 For the lead-time of 1-year, for some models only scattered predictive skill (> 95%
181 significance) in forecasting September sea ice concentration anomalies are found, generally in
182 the arc around the periphery of the Arctic Basin extending from north of Alaska to northeast of
183 Siberia (top panel of Fig. 3). The MMEE shows small clustered areas of significant ACCs
184 between the Beaufort and eastern Siberian Seas, whereas areas near the central Arctic Ocean has
185 the least predictive skill (negative ACCs, Fig. 3l in the top panel). In general, the areas of
186 significant ACCs in CCSM4, MIROC5 and MPI-ESM-MR are similar to that of the MMEE.

187 For the lead-time of 3-5 years, the areas of significant predictive skill become broader for
188 the majority of the models compared to those of 1-year, covering large parts of the northern
189 Beaufort, Chukchi, eastern Siberian and Laptev Seas (bottom panel of Fig. 3). The exceptions are
190 CFSv2 and GEOS-5. CFSv2 has too little sea ice cover in the Arctic Ocean due to the
191 aforementioned drift problem. The ACCs of GEOS-5 for the lead-time of 3-5 year are even
192 smaller than those of 1-year for the area of ACCs exceeding the 95% confidence level. The
193 MMEE shows large clustered areas of significant ACCs in the arc around the Arctic Basin
194 extending from north of Alaska to north of Siberia (Fig. 3l in the bottom panel). Again, the
195 central Arctic Ocean towards the Canadian Archipelago and northern Greenland Sea shows the
196 least predictive skill.

197 The results for the lead-time of 6-8 years are broadly similar to those of the lead-time of 3-5
198 years, although the areas of significant predictive skill are relatively broader for the majority of
199 the models (not shown). The MMEE also shows enlarged areas of significant ACCs relative to



200 those of 3-5 year, i.e., along the eastern coast of the Greenland (not shown). Overall, the MMEE
201 has better prediction skill relative to individual models for all lead times, although the MMEE
202 does not universally outperform every single constituent models.

203 Figure 4 shows the predicted trend (slope of a linear regression) as a function of lead times
204 after applying a 3-year average to filter out high frequency variability. For each individual model,
205 the trend is calculated based on its ensemble mean (see No. of ensemble members in Table 1).
206 All the models reproduce the observed negative trend, except that BCC-CSM1.1 has positive
207 trend at the lead-time of 1-3 and 2-4 years. However, the simulated negative trends show very
208 different magnitude, ranging from about -0.2 to -0.9×10^6 km² per decade. Compared to the
209 observation, there is a systematic underestimation of the decreasing trend throughout the
210 integration period for all decadal hindcasts. This is particularly true for the lead-time of 6-8 and
211 7-9 years (i.e., about -0.6×10^6 km² per decade for the MMEE vs. -1.2×10^6 km² per decade for the
212 observation), because those longer lead times are weighted towards inclusion of more recent
213 years in the observations with accelerated decline of Arctic sea ice.

214 To figure out to what extent the identified areas with significant ACCs at different lead times
215 are caused by the decadal decreasing trend, we remove the linear trend in the predicted and
216 observed sea ice concentration in each grid box. As shown in Fig. 5, after the trend is removed,
217 the areas with significant ACCs become much smaller relative to those of Fig. 3, especially for
218 the lead-time of 3-5 and 6-8 years. This suggests that high predictability found in Fig. 3 at longer
219 time scales is largely due to the decreasing Arctic sea ice in recent decades. Thus the relatively
220 long prediction skill over the areas of the northern Beaufort, Chukchi, eastern Siberian and
221 Laptev Seas is influenced by long-term sea ice reduction.



222 To further examine the prediction skill of Arctic sea ice variability in the context of regional
223 climate variability, we generate three sea ice extent indices: 1) the entire Arctic, 2) the north
224 Pacific, and 3) the north Atlantic. Sea ice variability in the north Pacific and north Atlantic is
225 modulated by different dominant decadal oscillations. Previous studies suggested that sea ice in
226 the Bering and Beaufort Seas is correlated with the Pacific Decadal Oscillation (PDO), which
227 has undergone a transition from a dominantly positive phase to a more negative phase in recent
228 decades (Lindsay and Zhang 2005; Zhang et al., 2010; Wendler et al., 2014). Sea ice in the north
229 Atlantic, particularly the ice export through Fram Strait and import from the Barents Sea, is
230 significantly affected by the phases of the North Atlantic Oscillation (e.g., Kwok, 2000; Rigor
231 and Wallace, 2004). Enfield et al. (2001) linked North Atlantic sea ice variability to the Atlantic
232 Multidecadal Oscillation (AMO) using the time frequency analysis of historical and paleo
233 records. Day et al. (2012) suggested that up to 30% of the north Atlantic sea ice decline during
234 1979-2010 might be attributed to the natural cycle of the AMO by analyzing five CMIP3 models.

235 Here we define the north Pacific sea ice index as the total September sea ice extent in the
236 Chukchi, East Siberian, and Laptev Seas (120°E-150°W and 62.5°N-80°N). The north Atlantic
237 sea ice index is defined as the total September sea ice extent in the Greenland, Norwegian, and
238 Barents Seas (40°W-80°E and 60°N-84°N, see boxes in Fig. 1). A 3-year average is also applied
239 to these indices.

240 The predictive skill for these indices is also measured by the anomaly correlation coefficient
241 between the model hindcast and observation. Figure 6 shows the ACC as a function of lead times
242 for the ensemble mean of each individual model and MMEE. To provide additional perspective
243 on the relative skill of the decadal experiments, the anomaly correlation coefficient of the
244 persistence prediction is also shown. Persistence prediction is the simplest way to produce a



245 forecast, which assumes sea ice state at the time of the forecast will not change. The horizontal
246 lines in Fig. 6 represent different confidence level. For the entire Arctic (Fig. 6a), the anomaly
247 correlation coefficient of most models exhibits certain predictive skill ($> 95\%$ significance),
248 except BCC-CSM1.1 for the lead-time of 1-3 and 2-4 years. Four models (CCSM4, FGOALS-g2,
249 GFDL-CM2.1 and MIROC5) show comparable or better predictive skill relative to the
250 persistence prediction for all the analyzed lead-times. The MMEE has more skillful results than
251 most of the individual model predictions during the entire period. The north Pacific sea ice index
252 has lower prediction skill and larger inter-model spread compared to those of the entire Arctic
253 index (Fig. 6c). In the north Pacific, only two models (GFDL-CM2.1 and MIROC5) show
254 comparable skill to the persistence prediction for the lead-time of 1-3 and 2-4 years. After 3-5
255 years, six models (CanCM4, CCSM4, FGOALS-g2, GFDL-CM2.1, MIROC5 and
256 MPI-ESM-MR) have better skill than the persistence prediction, which is also the case for the
257 MMEE. In general, the predictive skill of the north Atlantic sea ice index is poor compared to
258 both the entire Arctic and north Pacific indices, particularly for the lead-time from 3-5 to 5-7
259 years (insignificant ACCs). However, we note that in the north Atlantic sector all the models
260 show better predictive skill than the persistence prediction for the first three lead-times.
261 Additionally, all the models, except CanCM4, appear to have a re-emerging predictive skill for
262 the north Atlantic sea ice after 6-8 years (Fig. 6e). Overall, the MMEE has more skillful results
263 than that of the persistence prediction.

264 After removing the linear trend (Fig. 6b, d, f), the predictive skill of the above indices
265 decreases dramatically with very large inter-model spread. The MMEE only shows more skillful
266 results than the persistence prediction between 3-5 and 5-7 years for the north Pacific index.

267 **3.2 Antarctic sea ice**



268 Here we apply the same analysis in section 3.1 for Antarctic sea ice. Figure 7 shows time
269 series of September sea ice extent from the 10-year hindcast for each individual model and the
270 observations during 1981-2015. FGOALS-g2, GEOS-5, and MIROC5 produce significantly less
271 sea ice compared to the observation for the entire period with GEOS-5 having the smallest sea
272 ice extent of all the models. BCC-CSM1.1, CanCM4, and HadCM3 produce more sea ice
273 relative to the observations. The sea ice extent simulated by CCSM4, CFSv2, GFDL-CM2.1,
274 IPSL-CM5A-LR and MPI-ESM-MR is comparable to the observations, but they cannot
275 reproduce the gradual increase of Antarctic sea ice in recent years (e.g., Comiso et al., 2011). As
276 in the Arctic, the models that use direct and indirect full-field initialization tend to drift towards
277 their modeled sea ice state within a few years of initialization.

278 Figure 8 shows the anomaly correlation coefficient of each individual model and MMEE for
279 the lead-time of 1 and 3-5 years. For the 1-year lead-time, small scattered areas with predictive
280 skill greater than 95% confidence level in the Southern Ocean are found in most models. The
281 location of these scattered areas differs by model, although the MMEE shows small clustered
282 areas of significant ACCs in the central Weddell Sea (top panel of Fig. 8). There is no
283 improvement for the predictive skill for most models and the MMEE as the lead-time increases
284 to 3-5 years (bottom panel of Fig. 8) and 6-8 years (not shown). Overall, the predictive skill of
285 the MMEE does not outperform most models for all the lead-times.

286 The observed and predicted trends for different lead times are shown in Fig. 9. The observed
287 trends are positive for all the lead-times, and increase to $\sim 0.35 \times 10^6 \text{ km}^2$ per decade as recent
288 years are considered. By contrast, most models show negative trends, i.e., BCC-CSM1.1 has
289 negative trends ranging from $-0.6 \times 10^6 \text{ km}^2$ to $-1 \times 10^6 \text{ km}^2$ per decade. CCSM4 and FGOALS-g2
290 have increasing trends before 3-5 year and 5-7 year leads, respectively, but decreasing trends



291 thereafter. CFSv2 shows increasing trends after 2-4 year leads. However, these three
292 positive-trending models cannot simulate the magnitude of observed positive trends.

293 Again, we remove linear trends in both the model hindcast and observation, and then
294 calculate the ACC. After the linear trend is removed, the areas having significant predictive skill
295 become broader for the majority of the models compared to those of the raw data (Fig. 10 vs. Fig.
296 8), particularly for the lead-time of 3-5 and 6-8 years. Moreover, most models and the MMEE
297 have good predictive skill in the Ross Sea. As indicated by the MMEE, much of Antarctica's
298 coast has poor predictive skill (negative ACCs, Fig. 8).

299 Here we generate three regional sea ice extent indices: 1) the entire Antarctic, 2) the
300 central-eastern south Pacific and 3) the south Atlantic. We define the central-eastern south
301 Pacific index as the total September sea ice extent in the eastern Ross, Bellingshausen and
302 Amundsen Seas (165°W-75°W and 50°S-80°S) and the south Atlantic index as the total
303 September sea ice extent in the Weddell Sea (60°W-0° and 50°S-75°S, see boxes in Fig. 1).

304 Figure 11 shows the anomaly correlation coefficient as a function of lead times for the
305 ensemble mean of each individual model, the MMEE and the persistence prediction. For the
306 entire Antarctic, none of models can predict the observed sea ice variability (i.e., their
307 simulations are negatively correlated with the observations), except for CCSM4 and
308 GFDL-CM2.1, which show significant prediction skill (> 95% significance) at the lead-time of
309 1-3 years (Fig. 11a). Moreover, the persistence prediction is superior to the prediction of each
310 individual model and the MMEE. For the central-eastern south Pacific index, almost all the
311 models show poor predictive skill for almost all the lead-times, although CFSv2, GFLD-CM2.1
312 and HadCM3 exhibit significant skill at 1-3, 2-4 and 4-6 years, respectively. Unlike the entire



313 Antarctic, the MMEE of the central-eastern south Pacific shows better skill than that of the
314 persistence prediction, although neither is statistically significant (Fig. 11c). For the south
315 Atlantic index (Fig. 11e), almost all the models also do not have predictive skill (the ACCs are
316 not statistically significant), although CCSM4 has significant skill at the lead-time of 5-7 years.
317 However, the MMEE shows surprisingly significant skill, much better than the persistence
318 prediction, at 6-8 years (> 95% significance).

319 After removing linear trends in Fig. 11a, c, e, we note that there is no obvious improvement
320 in predictive skill for the entire Antarctic and the central-eastern south Pacific indice, but the
321 inter-model spread is increased (Fig. 11b, d). It is also noted that for the south Atlantic index, the
322 MMEE shows significant skill after 4-6 years (Fig. 11f).

323 **4. Discussion and conclusion**

324 This assessment provides a snapshot of the interannual to decadal predictability of sea ice in
325 the Arctic and Antarctic for the current-day coupled global climate models as part of the CMIP5
326 decadal prediction experiment.

327 Our evaluation shows that for many models, there are substantial discrepancies between the
328 decadal hindcast and observed September sea ice extent. For instance, in the Arctic, as
329 mentioned previously, CFSv2 dramatically underestimates September sea ice cover, leading to
330 pronounced drift in the first three years of the decadal hindcast. In contrast, CFSv2 simulates a
331 larger March sea ice extent ($2-3 \times 10^6$ km² more than the observation, not shown). Hence there is
332 an excessive melt of sea ice through the melting season which is due to not only the
333 underestimate of observed September sea ice cover, but also the overestimate of observed March
334 sea ice cover (March minus September). Such large errors have the potential to propagate



335 through other components of the climate system. This excessive melt greatly increases
336 freshwater in the Arctic Ocean and export of fresh water through Fram Strait into the northern
337 Atlantic. Following Koenigk et al. (2007), we calculate the freshwater export through Fram strait
338 using the following formula:

$$Q = \int_{z=B}^T \int_{x=x_0}^{x_1} u \left(\frac{S_{ref} - S}{S_{ref}} \right) dx dz$$

339 where B is the bottom of the ocean layer (here B = 100m), T is ocean surface; x0 and x1 are end
340 points of the selected cross-section (here the cross-section is along 74°N and between 30°W and
341 10°E); S, Sref are salinity and reference salinity (Sref = 34.8 psu). As shown in Fig. 12, there is a
342 pronounced increase of the freshwater export through Fram Strait into the northern Atlantic
343 during the first 4 years of integration, although the amount of the freshwater export decreases
344 gradually after that. Such freshwater propagation into the North Atlantic results in a weakening
345 of deep water formation in the Greenland Sea. Also shown in Fig. 12, the volume transport of the
346 Atlantic Meridional Overturning Circulation (AMOC) at 40°N in CFSv2 (which is too weak at
347 the beginning of the integration) decreases substantially during the decadal hindcast (4Sv after
348 10-year integration), which is a factor of 3-4 smaller than the observation (18.7Sv in
349 Cunningham et al., 2007; 17.2Sv in Smeed et al., 2014; McCarthy et al., 2015). Thus incorrect
350 prediction of sea ice in the Arctic could influence the AMOC prediction, which is a key source of
351 decadal predictability for European climate (Jackson et al., 2015), and has global impacts at
352 longer timescales.

353 It is well-known that brine rejection during sea ice growth strongly influences the formation
354 of the Antarctic Bottom Water (AASW). In the Antarctic, as mentioned previously, GEOS-5
355 simulates much less September sea ice extent, a factor of about 6 less than the observation,



356 which is also the case for March sea ice extent (not shown). The underestimation of sea ice
357 coverage might result in insufficient brine rejection through the freeze-up period in the GEOS-5.
358 This insufficient brine rejection is due to not only the underestimate of observed September sea
359 ice cover alone, but also the underestimate of observed March sea ice cover. Export of AABW
360 constitutes a key component of the meridional overturning circulation in the Southern Ocean
361 (Lumpkin and Speer 2007). The systematic underestimation of sea ice coverage results in a
362 weaker Deacon Cell in the Southern Ocean (~4Sv, Fig. 13) compared to the estimate of 20Sv
363 from Döös et al. (2007). Therefore, models that have large biases in simulating sea ice extent
364 (e.g., CFSv2 for the Arctic, GEOS-5 for the Antarctic) result in degraded predictive skill in sea
365 ice as well as other variables.

366 By performing the anomaly correlation analysis, we found that in the Arctic most models
367 only show small clustered areas with significant predictive skill at the lead-time of 1-year. As the
368 lead-time increases, for most models, the areas with significant predictive skill expand, covering
369 much of the northern Beaufort, Chukchi, eastern Siberian, and Laptev Seas. Such expansion is
370 largely due to the fact that almost all the models can predict observed negative trends of Arctic
371 sea ice, although the magnitude of the trend simulated by most models is still smaller than
372 observed. After the linear trend is removed, the areas with significant predictive skill at longer
373 time scales shrink greatly.

374 The analysis of regional indices suggests that sea ice in the Atlantic side has lower
375 predictability than that of the Pacific side. This is perhaps counterintuitive, since the AMO is
376 well predicted compared to the PDO (Kim et al., 2012). We do note that, for the Atlantic side of
377 the Arctic, most models show re-emerging predictive skill at the lead-time of 6-8 years. This
378 might be associated with the existence of interior AMOC pathways. A stronger (weaker) AMOC



379 results in warming (cooling) in the subpolar gyre after several years, contributing to enhanced
380 decadal predictability of sea ice in the north Atlantic sector (e.g., Mahajan et al. 2011; Zhang and
381 Zhang, 2015). In contrast to our results focusing on September sea ice, some idealized modeling
382 studies (Koenigk and Mikolakewicz 2009; Koenigk et al., 2012), which assess predictive skills
383 relative to their model climate, suggested annual and decadal mean sea ice concentration has
384 higher potential predictability for the Atlantic side than that of the Pacific side. Germe et al.
385 (2014) showed that the potential predictability of the winter Arctic sea ice extent comes mainly
386 from the Atlantic sector, while the Pacific sector seems unpredictable beyond the first year.
387 Further research is needed to explore the differences across model configurations.

388 By contrast, Antarctic sea ice does not show promising predictive skills at longer time scales.
389 Unlike in the Arctic counterpart, there is no obvious change in the areas showing significant
390 predictive skill as the lead-time increases. This might be because most models cannot predict
391 observed increasing Antarctic sea ice in recent decades. Instead almost all decadal hindcasts
392 predict a decrease of Antarctic sea ice, which is also true for the simulation in recent decades and
393 in response to forced simulations that include increased greenhouse gases in the atmosphere (e.g.,
394 Liu and Curry, 2010; Turner et al., 2013; Shu et al., 2015). Further investigating a range of other
395 variables such as simulated sea ice thickness, sea ice velocity, near surface wind, and ocean
396 stratification will help elucidate the reasons why the trends in these models are different from
397 observations. However, after the trend is removed, most models suggest that large parts of the
398 eastern south Pacific do have some predictive skill. Previous studies (e.g., Liu et al., 2002) have
399 showed that the intensification of the Hadley Circulation in the eastern equatorial Pacific during
400 El Nino leads to an equatorward shift of the storm track in the eastern south Pacific. This leads to
401 the changes of the regional Ferrel Circulation in the eastern Pacific, which cause an anomalous



402 poleward mean meridional heat flux into the sea ice zone in the eastern south Pacific and limits
403 sea ice growth there. Thus, relatively good sea ice predictability in the eastern south Pacific
404 might be related to the ENSO teleconnection. Holland and Raphael (2006) further showed that a
405 number of climate models have the ability in simulating the observed ENSO teleconnection in
406 sea ice in the eastern south Pacific and Atlantic. The analysis of regional indices suggests that the
407 MMEE has skillful results in the south Atlantic beyond 4-6 years, whether or not the trend is
408 removed.

409 An issue in this assessment is the relatively small sample size because of the limited number
410 of start years of the decadal prediction experiment. To promote both the science and practice of
411 decadal prediction, the CMIP phase 6 recommends ensembles of 10-year hindcast/prediction for
412 all years from 1960 to the end of the CMIP6 period (10 members recommended), which will be
413 helpful to obtain better statistics. As demonstrated in this study and previous studies, large biases
414 in models strongly influence sea ice prediction at decadal time scales. Thus continued efforts are
415 needed to identify, understand and reduce model errors, i.e., Kharin et al. (2012) demonstrated a
416 technique to correct non-linear drifts in decadal hindcasts. Some multi-model studies put efforts
417 on this issue for some climate variables (e.g., Bellucci et al., 2014; Doblas-Reyes et al., 2013;
418 Goddard et al., 2012).

419 Recent studies suggested that different initialization approaches and the density of
420 observations used in the initialization significantly affect the predictability of sea ice. Zunz et al.
421 (2015) tested three initialization approaches and found that the spread of ensembles at decadal
422 time scales can be reduced when more complicated data assimilation procedures and denser
423 observations are used to initialize the hindcasts. To date, only limited models have implemented
424 initialization of sea ice concentration (see Table 1 for details). Moreover, to better predict sea ice,



425 the accurate sea ice initialization requires not only sea ice concentration, but also variables (i.e.
426 sea ice thickness) influence surface energy fluxes and, thereby, ocean-atmosphere interaction. At
427 seasonal timescales, the initialization of sea ice thickness has been shown to be crucial for
428 summer prediction (e.g., Day et al. 2014b). Some studies (e.g., Blanchard-Wrigglesworth et al.
429 2011a; Koenigk and Mikolajewicz, 2009) suggested that the persistence of sea ice thickness
430 anomalies is much higher than that of sea ice concentration anomalies. Higher predictability of
431 Arctic sea ice thickness (volume) with respect to that of Arctic sea ice cover has been found at
432 longer time scales (e.g., Guemas et al., 2014). However, sea ice thickness has not yet been
433 initialized in CMIP5 models because of sparse observations. In this assessment, based on Table 1,
434 11 CMIP5 models can be separated into two groups: direct and indirect sea ice initialization. The
435 direct initialization includes CanCM4, CFSv2 and GEOS-5. Other models are indirect
436 initialization. Based on this division, we cannot conclude that the models initialized directly has
437 better performance on predictive skills compared to those initialized indirectly. CanCM4 has
438 broader area with significant predictive skill at longer lead-times (Figure 3). Its predictive skill is
439 better than some models (e.g., BCC-CSM1.1, HadCM3, IPSL-CM5A-LR), comparable with
440 CCSM4 and GFDL-CM2.1, but worse than MIROC5 and MMEE. On the other hand, CFSv2 has
441 strong model drift so that the predicted sea ice is substantially less than the observations.
442 GEOS-5 has nearly no skill on predicting observed sea ice variability. From this comparison, it is
443 not clear whether direct sea ice initialization is better than indirect sea ice initialization. Other
444 processes important for simulating sea ice evolution include the ocean below sea ice (i.e.,
445 temperature and salinity), which, due to its long persistence time, provides constraints on
446 predictions of sea ice at longer time scales. Thus, efforts should be devoted to further
447 development of initialization of the Arctic Ocean and Southern Ocean, which requires sufficient



448 observations and improved assimilation methods.

449 **Acknowledgements**

450 This research is supported by the NOAA Climate Program Office (NA14OAR4310216) and the
451 NSFC (41176169).

452 **5. References**

453 Bellucci, A. et al.: An assessment of a multi-model ensemble of decadal climate predictions.
454 *Clim. Dyn.* doi:10.1007/s00382-014- 2164-y, 2014.

455 Bindoff, N. L., and Coauthors: Detection and attribution of climate change: From global to
456 regional, in *Climate Change 2013: The Physical Science Basis. Contribution of Working Group I*
457 *to the Fifth Assessment Report of the Intergovernmental Panel on Climate Change*, edited by T.
458 F. Stocker et al., p. 908, Cambridge Univ. Press, Cambridge, U. K., and New York, 2013.

459 Blanchard-Wrigglesworth, E., Armour, K., Bitz, C. M. and deWeaver, E.: Persistence and
460 inherent predictability of Arctic sea ice in a GCM ensemble and observations. *J. Climate*, 24,
461 231–250, doi:10.1175/2010JCLI3775.1, 2011a.

462 Blanchard-Wrigglesworth E, Bitz, C. M. and Holland, M. M.: Influence of initial conditions and
463 climate forcing on predicting Arctic sea ice. *Geophys. Res. Lett.*, 38, L18503, 2011b.

464 Boé, J. L., Hall, A. and Qu, X.: September sea-ice cover in the Arctic Ocean projected to vanish
465 by 2100. *Nature Geosci.*, 2, 341–343, 2009.

466 Cavalieri, D. J. and Parkinson, C. L.: Arctic sea ice variability and trends, 1979-2010.
467 *Cryosphere*, 6, 881-889, 2012.



- 468 Collins, M., and Allen, M. R.: On assessing the relative roles of initial and boundary conditions
469 in interannual to decadal climate predictability, *J. Climate*, 21, 3104–3109, 2002.
- 470 Comiso, J. C. 2000, updated 2015: Bootstrap Sea Ice Concentrations from Nimbus-7 SMMR and
471 DMSP SSM/I-SSMIS. Version 2. Boulder, Colorado USA: NASA National Snow and Ice Data
472 Center Distributed Active Archive Center.
- 473 Comiso, J. C.: Large Decadal Decline of the Arctic Multiyear Ice Cover. *J. Climate*, 25,
474 1176–1193, 2012.
- 475 Comiso, J. C., Parkinson, C. L., Gersten, R. and Stock, L.: Accelerated decline in the Arctic sea
476 ice cover. *Geophys. Res. Lett.*, Vol. 35, L01703, doi: 10.1029/2007GL031972, 2008.
- 477 Comiso, J. C., Kwok, R., Martin, S. and Gordon, A. L.: Variability and trends in sea ice extent
478 and ice production in the Ross Sea. *J. Geophys. Res. Oceans*, 116, C04021, 2011.
- 479 Cunningham, S. A., Kanzow, T., Rayner, D., Baringer, M. O., Johns, W., Marotzke, E. J.,
480 Longworth, H. R., Grant, E. M., Hirschi, J. J.-M., Beal, L. M., Meinen, C. S., and Bryden, H. L.:
481 Temporal variability of the Atlantic meridional overturning circulation at 26.5N. *Science*, 317,
482 935–938, 2007.
- 483 Day, J. J., Hargreaves, J. C., Annan, J. D., and Abe-Ouchi, A.: Sources of multi-decadal
484 variability in Arctic sea ice extent. *Environ. Res. Lett.*, 7, 034011, 2012.
- 485 Day, J. J., Hawkins, E. and Tietsche, S. 2014a: Will Arctic sea ice thickness initialization
486 improve seasonal forecast skill? *Geophys. Res. Lett.*, 41, 7566–7575,
487 doi:10.1002/2014GL061694.



- 488 Day, J. J., Tietsche, S., and Hawkins, E. 2014b: Pan-arctic and regional sea ice predictability:
489 Initialization month dependence. *J. Climate*, 27, 4371–4390.
- 490 Day, J. J., Tietsche, S., Collins, M., Goessling, H. F., Guemas, V., Guillory, A., Hurlin, W. J.,
491 Ishii, M., Keeley, S. P. E., Matei, D., Msadek, R., Sigmond, M., Tatebe, H. and Hawkins, E.: The
492 Arctic Predictability and Prediction on Seasonal-to-Interannual Timescales (APPOSITE) data
493 set, *Geosci. Model Dev. Discuss.*, 8(10), 8809–8833, doi:10.5194/gmdd-8-8809-2015, 2015.
- 494 Doblas-Reyes, F. J., Andreu-Burillo, I., Chikamoto, Y., García-Serrano, J., Guemas, V., Kimoto,
495 M., Mochizuki, T., Rodrigues, L. R. L. and van Oldenborgh, G. J.: Initialized near-term regional
496 climate change prediction, *Nat. Commun.*, 4, 1715, doi:10.1038/ncomms2704, 2013.
- 497 Döös, K., Nycander, J. and Coward, A. C.: Lagrangian decomposition of the Deacon Cell. *J.*
498 *Geophys. Res.*, 113, C07028, doi:10.1029/2007JC004351, 2008.
- 499 Enfield, D. B., Mestas-Núñez, A. M. and Trimble, P. J.: The Atlantic Multidecadal Oscillation
500 and its relation to rainfall and river flows in the continental US. *Geophys. Res. Lett.*, 28,
501 2077–2080, 2001.
- 502 Fetterer, F., Knowles, K. Meier, W. and Savoie, M.: Sea ice index, digital media, National Snow
503 and Ice Data Center, Boulder, CO, 2002.
- 504 Fetterer, F., Knowles, K. Meier, W. and Savoie, M.: Sea ice index, digital media, National Snow
505 and Ice Data Center, Boulder, CO, 2010.
- 506 Francis, J. A., and Vavrus, S. J.: Evidence linking Arctic amplification to extreme weather in
507 mid-latitudes. *Geophys. Res. Lett.*, 39, L06801, doi:10.1029/2012GL051000, 2012.



- 508 Germe, A., Chevallier, M., Salas y Mélia, D., Sanchez-Gomez, E., and Cassou, C.: Interannual
509 predictability of Arctic sea ice in a global climate model: Regional contrasts and temporal
510 evolution. *Climate Dyn.*, 43, 2519–2538, doi:10.1007/s00382-014-2071-2, 2014.
- 511 Goddard, L., Kumar, A., Solomon, A., Smith, D., Boer, G., Gonzalez, P., Kharin, V., Merryfield,
512 W., Deser, C., Mason, S. J., Kirtman, B. P., Msadek, R., Sutton, R., Hawkins, E., Fricker, T.,
513 Hegerl, G., Ferro, C. A. T., Stephenson, D. B., Meehl, G. A., Stockdale, T., Burgman, R., Greene,
514 A. M., Kushnir, Y., Newman, M., Carton, J., Fukumori, I. and Delworth, T.: A verification
515 framework for interannual-to-decadal predictions experiments, *Clim. Dyn.*,
516 doi:10.1007/s00382-012-1481-2, 2012.
- 517 Goosse, H., Close, S., Dubinkina, S., Massonnet, F., Zunz, V., Vannitsem, S., Schaeybroeck, B.
518 V., Barth, A., and Canter, M.: Understanding and predicting Antarctic sea ice variability at the
519 decadal timescale, PREDANTAR, 2015.
- 520 Guemas, V., et al.: A review on Arctic sea ice predictability and prediction on
521 seasonal-to-decadal timescales, *Q. J. R. Meteorol. Soc.*, doi:10.1002/qj.2401, 2014.
- 522 Holland, M. M., and Raphael, M. N.: Twentieth century simulation of the Southern Hemisphere
523 climate in coupled models. Part II: Sea ice conditions and variability. *Clim. Dyn.*, 26, 229–245,
524 2006.
- 525 Holland, M. M., Bailey, D.A., and Vavrus, S.: Inherent sea ice predictability in the rapidly
526 changing Arctic environment of the Community Climate System Model, version 3, *Clim. Dyn.*,
527 36, 1239-1253, 2011.



- 528 Holland, M. M., Blanchard-Wrigglesworth, E., Kay, J., and Vavrus, S.: Initial-value
529 predictability of Antarctic sea ice in the Community Climate System Model 3, *Geophys. Res.*
530 *Lett.*, doi:10.1002/grl.50410, 2013.
- 531 Ishii, M., and Kimoto, M.: Reevaluation of historical ocean heat content variations with
532 time-varying XBT and MBT depth bias corrections. *J. Oceanogr.*, 292 *Journal of the*
533 *Meteorological Society of Japan* Vol. 90A65, 287–299, 2009.
- 534 Jackson, L. C., Kahana, R., Graham, T., Ringer, M. A. Woollings, T., Mecking, J. V., and Wood,
535 R. A.: Global and European climate impacts of a slowdown of the AMOC in a high resolution
536 GCM. *Clim. Dyn.*, Online Publish, 2015.
- 537 Jeffries, M. O., Richter-Menge, J., and Overland, J. E., (Eds.): *Arctic Report Card 2015*,
538 <http://www.arctic.noaa.gov/reportcard> , 2015.
- 539 Jung, T., Gordon, N., Klebe, S., Bauer, P., Bromwich, D. H., Day, J., Doblas-Reyes, F., Fairall,
540 C., Hines, K., Holland, M., Iversen, T., Lemke, P., Mills, B., Nurmi, P., Renfrew, I., Smith, G.,
541 Svensson, G., Tolstykh, M.: ‘WWRP Polar Prediction Project implementation plan’.
542 WWRP/PPP No.2. <http://polarprediction.net/en/documents/> (accessed 29 August 2014), 2013.
- 543 Kattsov, V., Ryabinin, V., Overland, J., Serreze, M., Visbeck, M., Walsh, J., Meier, W., and
544 Zhang, X.: Arctic sea ice change: A grand challenge of climate science, *J. Glaciol.*, 56(200),
545 1115–1121, doi:10.3189/002214311796406176, 2010.
- 546 Keenlyside, N. S., Latif, M., Jungclaus, J., Kornblueh, L., and Roeckner, E.: Advancing
547 decadal-scale climate prediction in the North Atlantic sector. *Nature*, 453, 84–88,
548 doi:10.1038/nature06921, 2008.



- 549 Kharin, V. V., Boer, G. J., Merryfield, W. J., Scinocca, J. F. and Lee, W.-S.: Statistical
550 adjustment of decadal predictions in a changing climate, *Geophys. Res. Lett.*, 39(19), n/a–n/a,
551 doi:10.1029/2012GL052647, 2012.
- 552 Kim, H.-M., Webster, P. J., and Curry, J. A.: Evaluation of short-term climate change prediction
553 in multi-model CMIP5 decadal hindcasts. *Geophys. Res. Lett.*, 39, L10701, 2012.
- 554 Koenigk, T. and Mikolajewicz, U.: Seasonal to interannual climate predictability in mid and high
555 northern latitudes in a global coupled model. *Clim. Dyn.* 32: 783-798, 2009.
- 556 Koenigk T., Mikolajewicz, U., Haak, H., and Jungclaus J.: Arctic Freshwater Export in the 20th
557 and 21st Century. *J. Geophys. Res.* 112:GS04S41. doi:10.1029/2006JG000274, 2007.
- 558 Koenigk, T., Beatty, C. K., Caian, M., Do'scher, R., and Wyser, K.: Potential decadal
559 predictability and its sensitivity to sea ice albedo parameterization in a global coupled model.
560 *Clim. Dyn.*, 38, 2389–2408, 2012.
- 561 Kurtz, N. T., and Markus, T.: Satellite observations of Antarctic sea ice thickness and volume, *J.*
562 *Geophys. Res.*, 117, C08025, doi:10.1029/2012JC008141, 2012.
- 563 Kwok, R.: Recent changes of the Arctic Ocean sea ice motion associated with the North Atlantic
564 Oscillation. *Geophys. Res. Lett.*, 27, 775–778, 2000.
- 565 Kwok, R., Cunningham, G. F., Wensnahan, M., Rigor, I., Zwally, H. J. and Yi, D.: Thinning and
566 volume loss of the Arctic Ocean sea ice cover: 2003–2008, *J. Geophys. Res.*, 114, C07005,
567 doi:10.1029/2009JC005312, 2009.



- 568 Lindsay, R. W., and Zhang, J.: The Thinning of Arctic Sea Ice, 1988–2003: Have We Passed a
569 Tipping Point?. *J. Clim.*, 18, 4879–4894, 2005.
- 570 Liu, J. F., Yuan, X., Rind, D., and Martinson, D.: Mechanism study of the ENSO and southern
571 high latitude climate teleconnections. *Geophys. Res. Lett.*, 29, 1679,
572 doi:10.1029/2002GL015143, 2002.
- 573 Liu, J., and Curry, J. A.: Accelerated warming of the Southern Ocean and its impacts on the
574 hydrological cycle and sea ice. *Proc. Natl. Acad. Sci. USA*, 107, 14 987–14 992, 2010.
- 575 Liu, J., Curry, J. A., and Martinson, D. G.: Interpretation of recent Antarctic sea ice variability.
576 *Geophys. Res. Lett.*, 31, L02205, doi:10.1029/2003GL018732, 2004.
- 577 Liu, J., Curry, J. A., Wang, H., Song, M., and Horton, R.: Impact of declining Arctic sea ice on
578 winter snowfall. *Proc. Natl. Acad. Sci. USA*, 109, 4074–4079; Corrigendum, 109, 6781–6783,
579 2012.
- 580 Liu, J., Song, M., Horton, R. M., and Hu, Y.: Reducing spread in climate model projections of a
581 September ice-free Arctic. *Proc. Natl. Acad. Sci. USA*, 110, 12 571–12 576,
582 doi:10.1073/pnas.1219716110, 2013.
- 583 Lumpkin, R., and Speer, K.: Global ocean meridional overturning. *J. Phys. Oceanogr.*, 37,
584 2550–2562, 2007.
- 585 Mahajan, S, Zhang, R. and Delworth, T. L.: Impact of the Atlantic Meridional Overturning
586 Circulation (AMOC) on Arctic surface air temperature and sea-ice variability. *J. Climate*, 24,
587 DOI:10.1175/2011JCLI4002.1, 2011.



- 588 Massonnet, F., Fichefet, T., Goosse, H., Bitz, C. M., Philippon-Berthier, G., Holland, M. M., and
589 Barriat, P. Y.: Constraining projections of summer Arctic sea ice. *Cryosphere*, 6, 1383–1394,
590 2012.
- 591 McCarthy, G. D., Smeed, D. A., Johns, W. E., Frajka-Williams, E., Moat, B. I., Rayner, D.,
592 Baringer, M. O., Meinen, C. S., and Bryden, H. L.: Measuring the Atlantic meridional
593 overturning circulation at 26°N, *Prog. Oceanogr.*, 130, 91–111, 2015.
- 594 Meehl, G. A. and Coauthors: Decadal Prediction. *Bull. Amer. Meteor. Soc.*, 90, 1467–1485. doi:
595 <http://dx.doi.org/10.1175/2009BAMS2778.1>, 2009.
- 596 Meehl, G. A., Hu, A., Arblaster, J. M., Fasullo, J., and Trenberth, K. E.: Externally Forced and
597 Internally Generated Decadal Climate Variability Associated with the Interdecadal Pacific
598 Oscillation. *J. Climate*, 26, 7298–7310. doi: <http://dx.doi.org/10.1175/JCLI-D-12-00548.1>, 2013
- 599 Merryfield, W. J., Lee, W-S., Boer, G. J., Kharin, V. V., Scinocca, J. F., Flato, G. M.,
600 Ajayamohan, R. S., Fyfe, J. C., Tang, Y., and Polavarapu, S.: The Canadian Seasonal to
601 Interannual Prediction System. Part I: Models and Initialization. *Mon. Wea. Rev.*, 141,
602 2910-2945, doi:10.1175/MWR-D-12-00216.1, 2013.
- 603 Mochizuki, T., Chikamoto, T., Kimoto, M., Ishii, M., Tatebe, H., Komuro, Y., Sakamoto, T.,
604 Watanabe, M., and Mori, M.: Decadal prediction using a recent series of MIROC global climate
605 models. *J. Meteor. Soc. Japan*, 90, 373–383, 2012.
- 606 Msadek, R., Vecchi, G. A., Winton, M., Gudgel, R. G.: Importance of initial conditions in
607 seasonal predictions of Arctic sea ice extent. *Geophys. Res. Lett.* DOI: 10.1002/2014GL060799,
608 2014.



- 609 Müller, W. A., Baehr, J., Haak, H., Jungclaus, J. H., Kröger, J., Matei, D., Notz, D., Pohlmann,
610 H., von Storch, J.-S., and Marotzke, J.: Forecast skill of multi-year seasonal means in the decadal
611 prediction system of the Max Planck Institute for Meteorology. *Geophys. Res. Lett.*, 39, L22707,
612 doi:10.1029/2012GL053326, 2012.
- 613 National Research Council. *Seasonal-to-Decadal Predictions of Arctic Sea Ice: Challenges and*
614 *Strategies*. Washington, DC: The National Academies Press, 2012.
- 615 Parkinson, C. L., and Cavalieri, D. J.: Antarctic sea ice variability and trends, 1979-2010. *The*
616 *Cryosphere*, 6, 871-880, 2012.
- 617 Pohlmann, H., Jungclaus, J. H., Köhl, A., Stammer, D., and Marotzke, J.: Initialized decadal
618 climate predictions with the GECCO oceanic synthesis: Effects on the North Atlantic. *J. Climate*,
619 22, 3926–3938, 2009.
- 620 Richter-Menge, J. A., and Coauthors: *Seasonal-to-Decadal Predictions of Arctic Sea Ice:*
621 *Challenges and Strategies*, National Academies Press, Washington, DC, 2012
- 622 Rigor, I. G., and Wallace, J. M.: Variations in age of Arctic sea ice and summer sea-ice extent.
623 *Geophys. Res. Lett.*, 31, L09401, 2004.
- 624 Serreze, M. C., Holland, M. M. and Stroeve, J.: Perspectives on the Arctic’s shrinking sea-ice
625 cover. *Science*, 315, 1533–1536, 2007.
- 626 Shu, Q., Song, Z., and Qiao, F.: Assessment of sea ice simulations in the CMIP5 models. *The*
627 *Cryosphere*, 9, 399-409, 2015.



- 628 Smeed, D. A., and Coauthors: Observed decline of the Atlantic Meridional Overturning
629 Circulation 2004–2012. *Ocean Sci.*, 10, 29–38, doi:10.5194/os-10-29-2014, 2014.
- 630 Smith, L. C., and Stephenson, S. R.: New Trans-Arctic shipping routes navigable y mid-century,
631 *Proc. Natl. Acad. Sci. U. S. A.*, 110(13), E1191–E1195, doi:10.1073/pnas.1214212110, 2013.
- 632 Smith, D. M., Cusack, S. A., Colman, W., Folland, C. K., Harris, G. R., and Murphy, J. M.:
633 Improved surface temperature prediction for the coming decade from a global climate model.
634 *Science*, 317, 796–799, 2007.
- 635 Stroeve, J., Holland, M. M., Meier, W., Scambos, T., and Serreze, M.: Arctic sea ice decline:
636 Faster than forecast. *Geophys. Res. Lett.*, 34, L09501, 2007.
- 637 Stroeve, J. C., Kattsov, V., Barrett, A., Serreze, M., Pavlova, T., Holland, M. M., and Meier, W.
638 N.: Trends in Arctic sea ice extent from CMIP5, CMIP3 and observations. *Geophys. Res. Lett.*,
639 39, L16502, 2012.
- 640 Stroeve, J. C., Hamilton, L. C., Bitz, C. M., and Blanchard-Wrigglesworth, E.: Predicting
641 September sea ice: Ensemble skill of the SEARCH Sea Ice Outlook 2008-2013. *Geophys. Res.*
642 *Lett.*, Vol. 41, 2014.
- 643 Stroeve, J. C., Markus, T., Boisvert, L., Miller, J., and Barrett, A.: Changes in Arctic melt season
644 and implications for sea ice loss, *Geophys. Res. Lett.*, 41, 1216–1225,
645 doi:10.1002/2013gl058951, 2014.
- 646 Taylor, K. E., Stouffer, R. J., and Meehl, G. A.: An overview of CMIP5 and the experiment
647 design. *Bull. Amer. Meteor. Soc.*, 93, 485–498, 2012.



- 648 Tietsche, S., Notz, D., Jungclaus, J. H. and Marotzke, J.: Predictability of large interannual
649 Arctic sea-ice anomalies, *Clim. Dyn.*, doi:10.1007/s00382-013-1698-8, 2013.
- 650 Tietsche, S., and Coauthors: Seasonal to interannual Arctic sea ice predictability in current global
651 climate models. *Geophys. Res. Lett.*, 41, 1035–1043, doi:10.1002/2013GL058755, 2014.
- 652 Turner, J., and Coauthors: Non-annular atmospheric circulation change induced by stratospheric
653 ozone depletion and its role in the recent increase of Antarctic sea ice extent. *Geophys. Res. Lett.*,
654 36, L08502, doi:10.1029/2009GL037524, 2009.
- 655 Turner, J., Bracegirdle, T. J., Phillips, T., Marshall, G. J., and Scott Hosking, J.: An initial
656 assessment of Antarctic sea ice extent in the CMIP5 models, *J. Clim.*, 26(5), 1473–1484, 2013.
- 657 Vera, C., and Coauthors: Needs assessment for climate information on decadal time scales and
658 longer. *World Climate Conference-3, Geneva, Procedia Environmental SciencesSwitzerland*, eds.
659 Sivakumar, M. et al., 1, 275-286, 2010.
- 660 Wang, M., and Overland, J. E.: A sea ice free summer Arctic within 30 years? *Geophys. Res.*
661 *Lett.*, 36, L07502, 2009.
- 662 Wang, M., and Overland, J. E.: A sea ice free summer Arctic within 30 years: An update from
663 CMIP5 models. *Geophys. Res. Lett.*, 39, L18501, 2012.
- 664 Wendler, G., Chen, L., and Moore, B.: Recent sea ice increase and temperature decrease in the
665 Bering Sea area, Alaska, *Theoretical and Applied Climatology*, 117, 393-398, 2014.
- 666 Zhang, X.: Sensitivity of Arctic summer sea ice coverage to global warming forcing: Towards
667 reducing uncertainty in arctic climate change projections. *Tellus A*, 62, 220–227, 2010.



668 Zhang, J., Woodgate, R., and Moritz, R.: Sea ice response to atmospheric and oceanic forcing in
669 the Bering Sea, *J. Phys. Oceanogr.*, 40, 1729–1747, doi:0.1175/2010JPO4323.1, 2010.

670 Zhang, J, and Zhang, R.: On the Evolution of Atlantic Meridional Overturning Circulation
671 (AMOC) Fingerprint and Implications for Decadal Predictability in the North Atlantic. *Geophys.*
672 *Res. Lett.*, 42(13), doi:10.1002/2015GL064596, 2015.

673 Zunz, V., Goosse, H., and Dubinkina, S.: Impact of the initialisation on the predictability of the
674 Southern Ocean sea ice at interannual to multi-decadal timescales. *Clim. Dyn.*, 44, 2267-2286,
675 2015.

676 **Figure Captions:**

677 Figure 1. Linear trends of September sea ice concentration for (a) Arctic and (b) Antarctic during
678 the period of 1979-2014. The meshed areas denote the trends above 95% confidence level. Boxes
679 indicate the areas used to generate the regional sea ice indices.

680 Figure 2. Time series of September Arctic sea ice extent (seasonal minimum) from the
681 simulations of the 10-year hindcast for each ensemble member of each individual model (thin
682 gray line), the ensemble mean of each individual model (thick red line) and satellite observation
683 (black line) from 1981 to 2015.

684 Figure 3. Anomaly correlation coefficients between the simulated and observed Arctic
685 September sea ice concentration anomalies for the lead-time of 1-year (top panel) and 3-5 years
686 (bottom panel). The correlation coefficient 0.61, 0.73 and 0.88 represents 90%, 95% and 99%
687 confidence levels, respectively.

688 Figure 4. The predicted trends (slope of a linear regression) of September Arctic sea ice extent
689 anomalies as a function of the lead-time after applying a 3-year average.



690 Figure 5 same as Figure 3, but for detrended September sea ice concentration anomalies.

691 Figure 6. Anomaly correlation coefficients between the simulated and observed Arctic
692 September sea ice extent anomalies for the three regional indices (the entire Arctic, Pacific and
693 Atlantic) as a function of the lead-time. The top and bottom panels are the original and detrended
694 time series, respectively. The horizontal dashed and solid lines represent 90%, 95% and 99%
695 confidence levels, respectively. The thick gray line is the persistence prediction.

696 Figure 7. Time series of September Antarctic sea ice extent (seasonal minimum) from the
697 simulations of the 10-year hindcast for each ensemble member of each individual model (thin
698 gray line), the ensemble mean of each individual model (thick red line) and satellite observation
699 (black line) from 1981 to 2015.

700 Figure 8. Anomaly correlation coefficients between the simulated and observed Antarctic
701 September sea ice concentration anomalies for the lead-time of 1-year (top panel) and 3-5 years
702 (bottom panel). The correlation coefficient 0.61 ,0.73 and 0.88 represents 90%, 95% and 99%
703 confidence levels, respectively.

704 Figure 9. The predicted trends (slope of a linear regression) of September Antarctic sea ice extent
705 anomalies as a function of the lead-time after applying a 3-year average.

706 Figure 10. same as Figure 8, but for detrended September sea ice concentration anomalies.

707 Figure 11. Anomaly correlation coefficients between the simulated and observed Antarctic
708 September sea ice extent anomalies for the three regional indices (the entire Antarctic, eastern
709 Pacific and Atlantic) as a function of the lead-time. The top and bottom panels are the original
710 and detrended time series, respectively. The horizontal dashed and solid lines represent 90%, 95%
711 and 99% confidence levels, respectively. The thick gray line is the persistence prediction.



712 Figure 12. (a) Freshwater export through Fram Strait (the cross-section along 74°N and between
713 30°W and 10°E), (b) Atlantic Ocean meridional overturning streamfunction in September
714 averaged for all decadal hindcasts from 1981 to 2015 for the CFSv2 (upper panel) and (c) time
715 series of stream function averaged over 40-55N, 500-1500m as indicated by the black in upper
716 panel (lower panel). The thin gray line represents each ensemble member and the thick black line
717 represents the ensemble mean.

718 Figure 13. Atlantic Ocean meridional overturning streamfunction in September averaged for all
719 decadal hindcasts from 1981-2015 for GEOS-5 (upper panel) and time series of stream function
720 averaged over 45-70N, 500-2000m as indicated by the black in upper panel (lower panel). The
721 thin gray line represents each ensemble member and the thick black line represents the ensemble
722 mean.

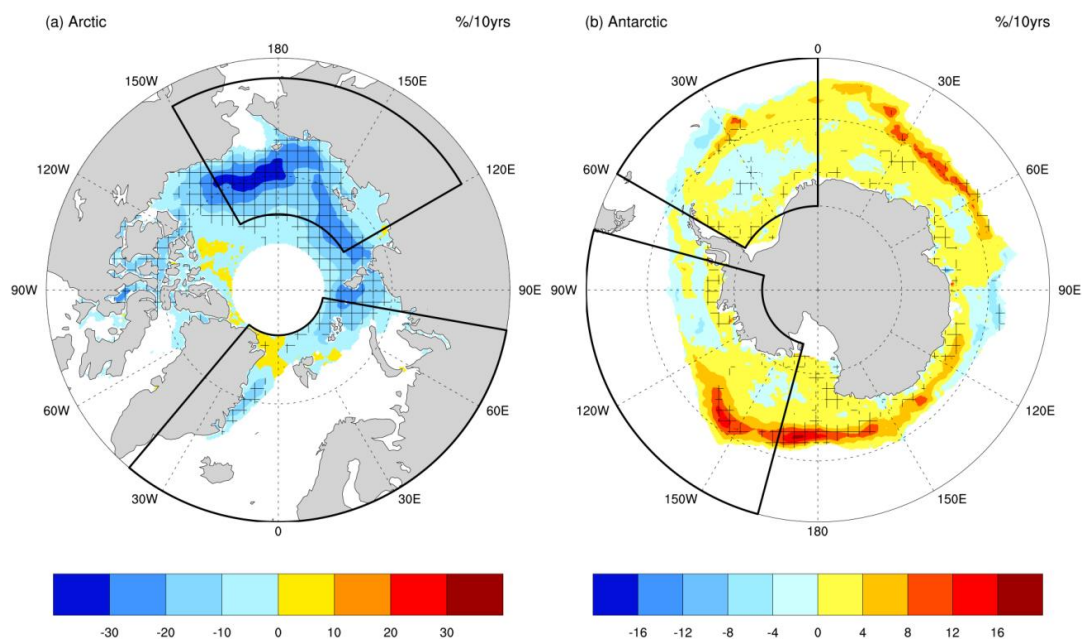
723



724 Table 1 Summary of initialization methods and data sources used for the CIMP5 decadal
 725 hindcast/prediction

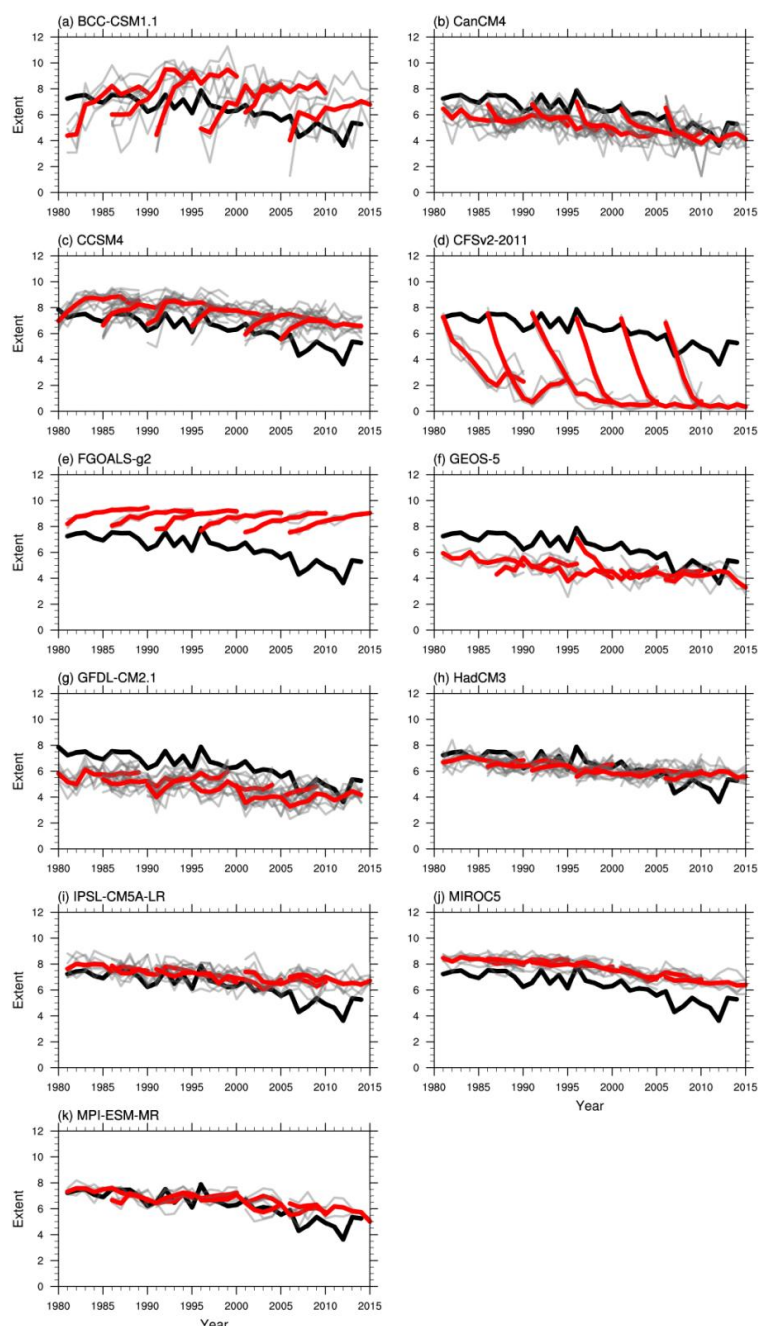
| Model | Resolution (sea ice model) | Ensemble members | Sea ice assimilation method and data source |
|--------------|----------------------------------|---------------------|---|
| BCC-CM1.1 | 1 lon x 1-1/3 lat | 4 | None, but the initial sea ice indirectly influenced by nudging T to SODA ocean reanalysis |
| CanCM4 | ~2.8 lon x 2.8 lat | 10 | Full-field using SIC from HadISST1.1 and SIT from model-based climatology (Merryfield et al., 2013) |
| CCSM4 | 0.9 lon x 1.25 lat | 10 | Full-field using bias-corrected CORE2-forced ocean hindcast |
| CFSv2 | 0.5 lon x 0.5 lat | 4 | Full-field using NCEP climate forecast system reanalysis |
| FGOALS-g2 | 1 lon x 1 lat | 3 | None, but the initial sea ice indirectly influenced by nudging T and S to an ocean reanalysis |
| GEOS-5 | 1 lon x 1 lat | 3 | Full-field using GEOS-iODAS |
| GFDL-CM2.1 | ~1 lon x 0.75 lat | 10 | None, but the initial sea ice indirectly influenced by atmospheric and ocean data (Msadek et al. 2014) |
| HadCM3 | 1.25 lon x 1.25 lat | 10 | Anomaly-field using Met Office Hadley Centre sea ice data (HadISST) |
| IPSL-CM5A-LR | ~2 lon x 2 lat | 6 | None, but the initial sea ice indirectly influenced by the assimilation of T and S anomalies from observations |
| MIROC5 | 1 lon x 1 lat | 6 | None, but the initial sea ice is indirectly influenced by the assimilation of T and S from an objective analysis of Ishii and Kimoto (2009) |
| MPI-ESM-MR | ~0.4 lon x 0.4 lat | 3 | None, but the initial sea ice indirectly influenced by the assimilation of T and S anomalies from a forced ocean run using NCEP reanalysis (Müller et al., 2012) |

726 SIC: sea ice concentration; SIT: sea ice thickness, T: ocean temperature, S: salinity



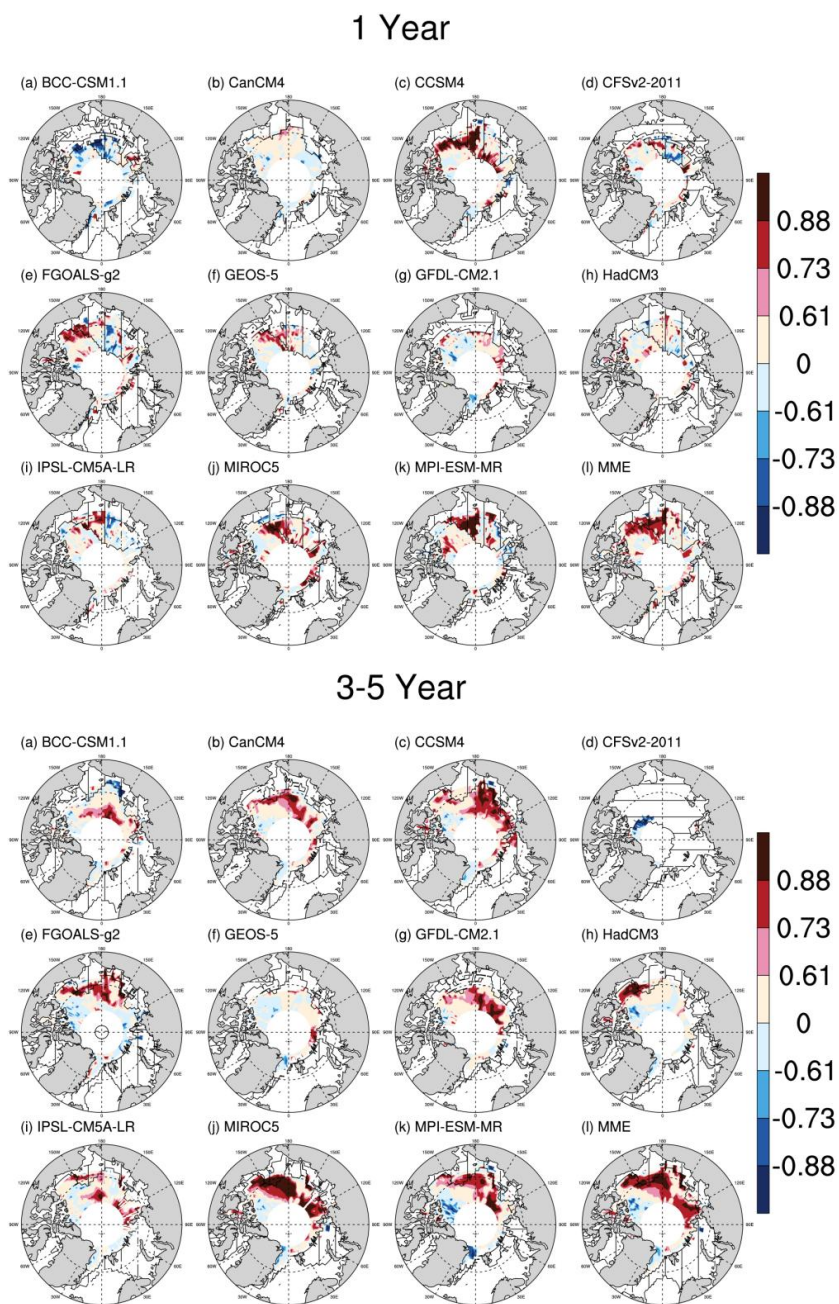
727
728
729
730
731

Figure 1. Linear trends of September sea ice concentration for (a) Arctic and (b) Antarctic during the period of 1979-2014. The meshed areas denote the trends above 95% confidence level. Boxes indicate the areas used to generate the regional sea ice indices.



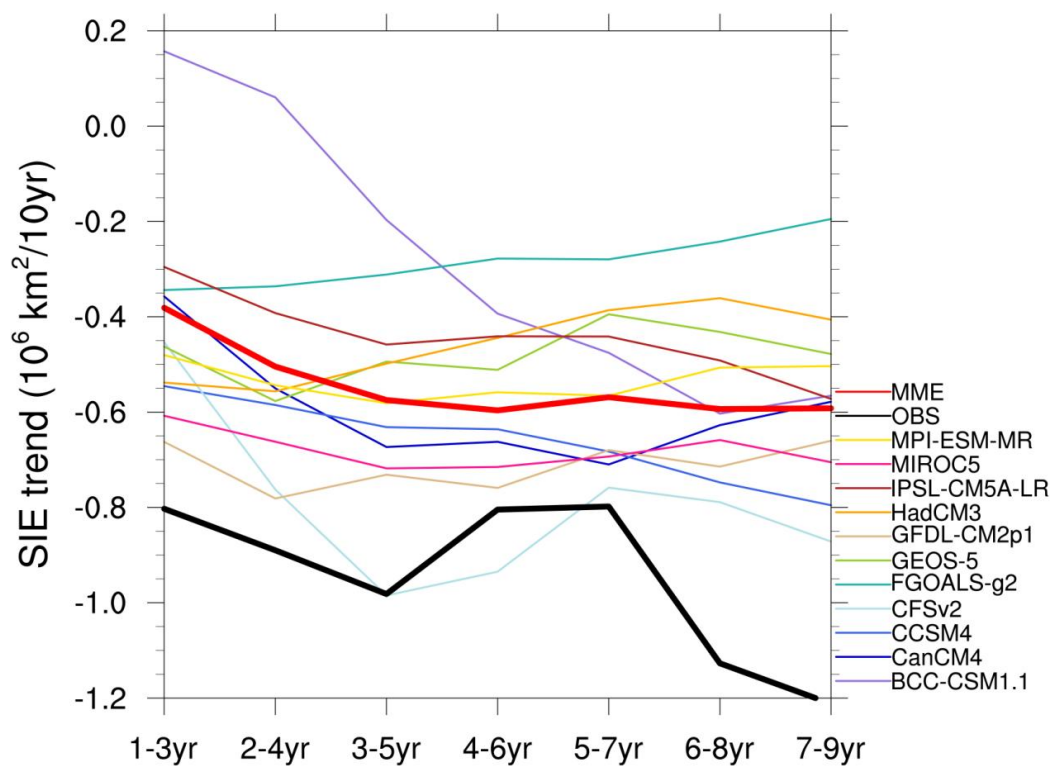
732

733 Figure 2. Time series of September Arctic sea ice extent (seasonal minimum) from the
734 simulations of the 10-year hindcast for each ensemble member of each individual model (thin
735 gray line), the ensemble mean of each individual model (thick red line) and satellite observation
736 (black line) from 1981 to 2015.



737

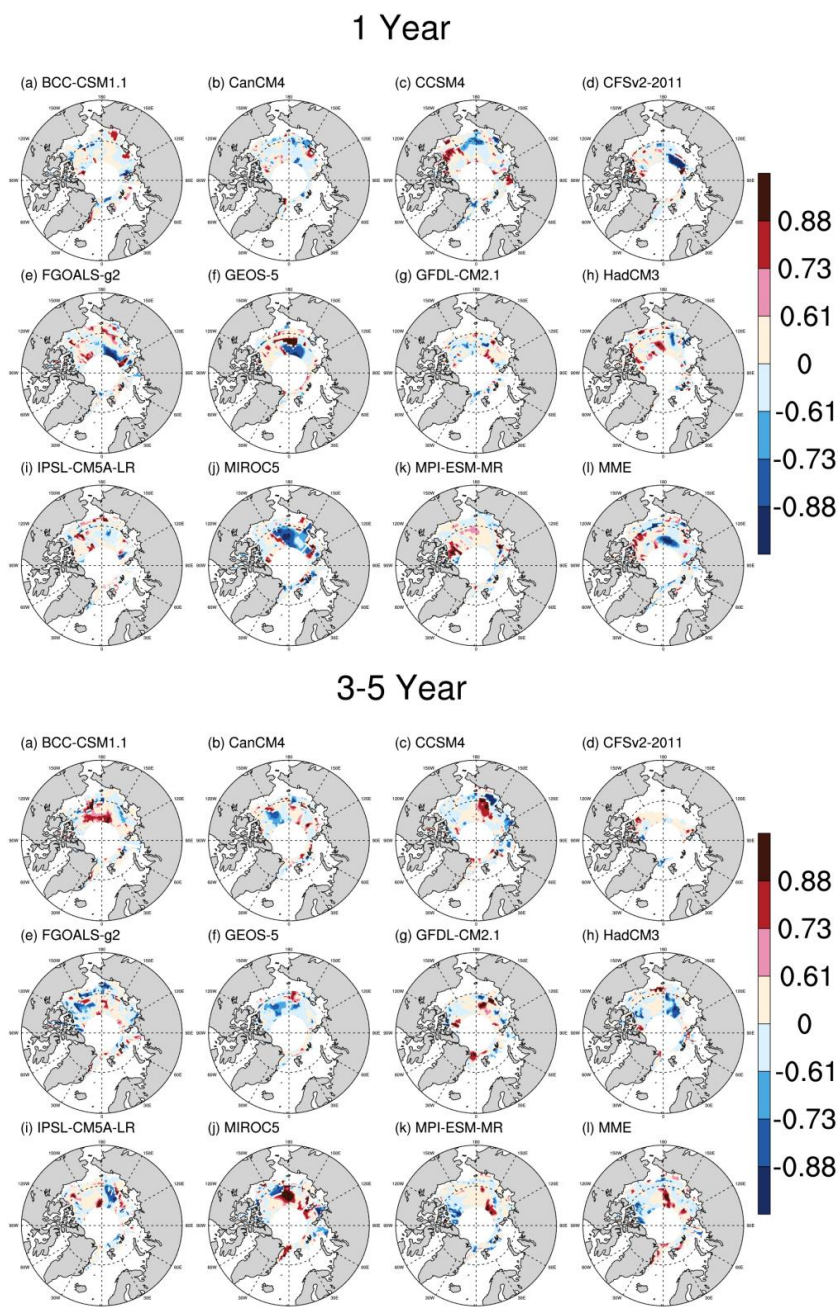
738 Figure 3. Anomaly correlation coefficients between the simulated and observed Arctic
 739 September sea ice concentration anomalies for the lead-time of 1-year (top panel) and 3-5 years
 740 (bottom panel). The correlation coefficient 0.61, 0.73 and 0.88 represents 90%, 95% and 99%
 741 confidence levels, respectively.



742

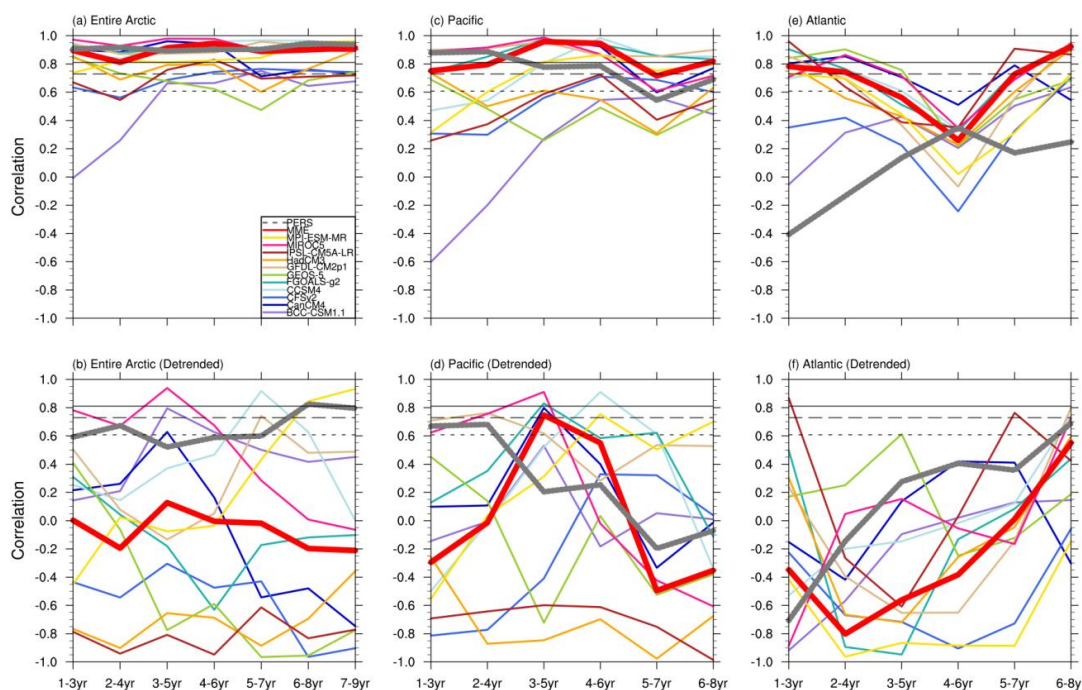
743 Figure 4. The predicted trends (slope of a linear regression) of September Arctic sea ice extent
744 anomalies as a function of the lead-time after applying a 3-year average.
745

745



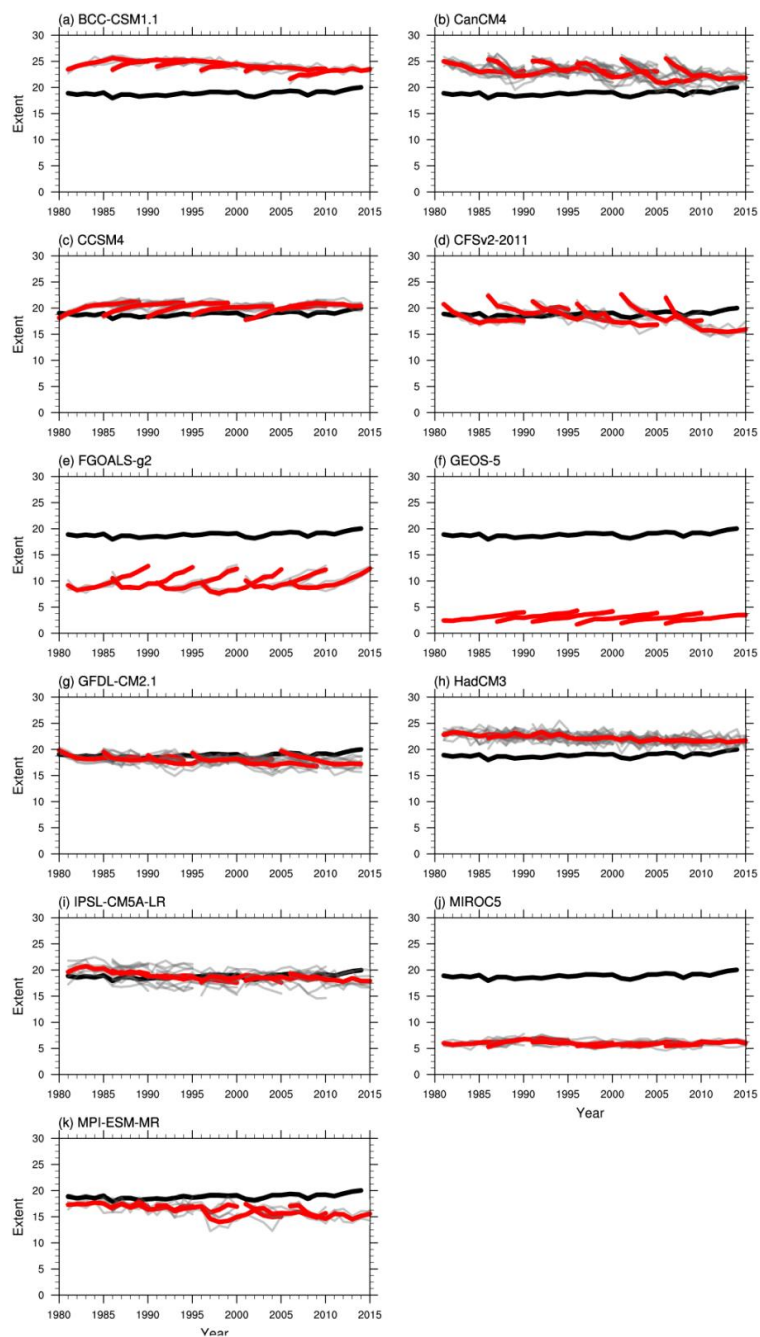
746

747 Figure 5 same as Figure 3, but for detrended September sea ice concentration anomalies.
748



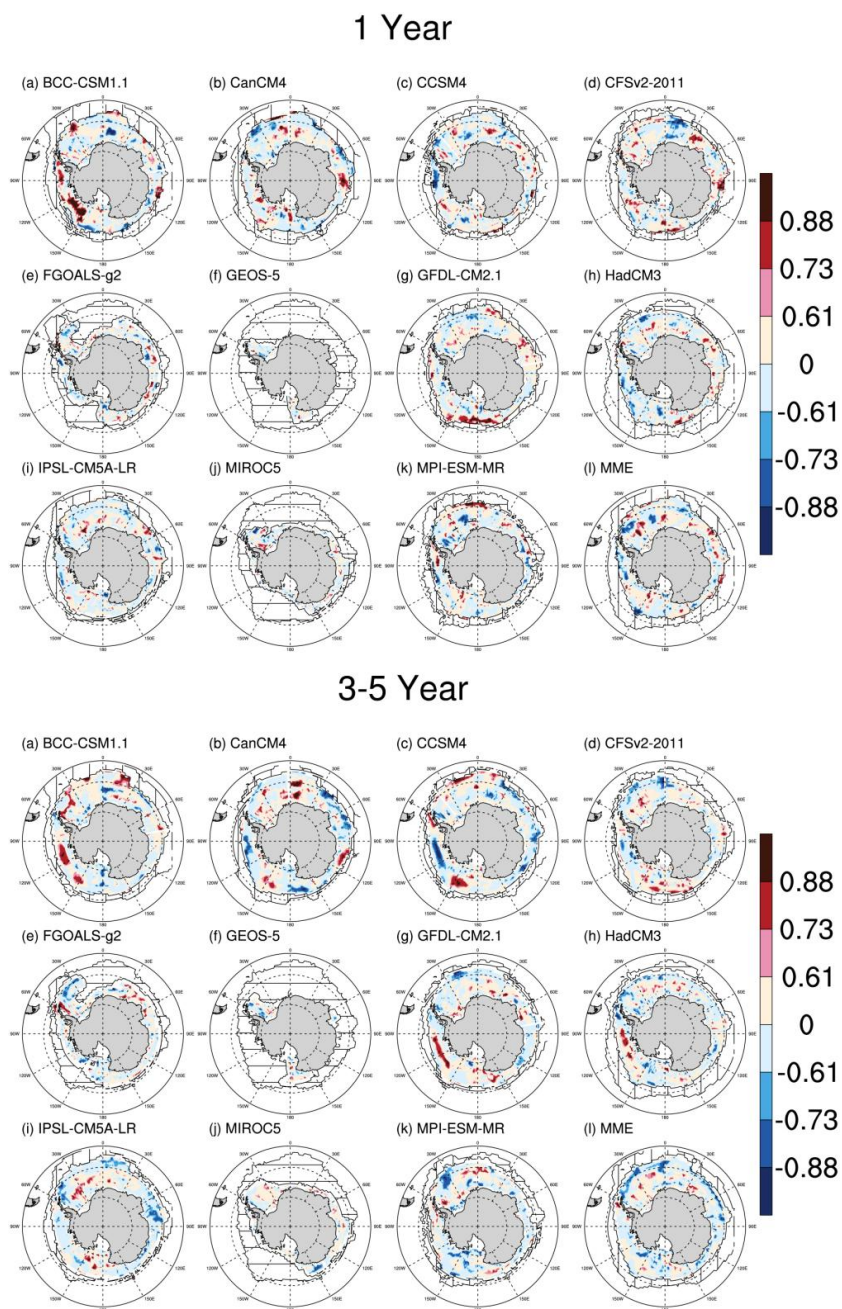
749

750 Figure 6. Anomaly correlation coefficients between the simulated and observed Arctic
 751 September sea ice extent anomalies for the three regional indices (the entire Arctic, Pacific and
 752 Atlantic) as a function of the lead-time. The top and bottom panels are the original and detrended
 753 time series, respectively. The horizontal dashed and solid lines represent 90%, 95% and 99%
 754 confidence levels, respectively. The thick gray line is the persistence prediction.
 755



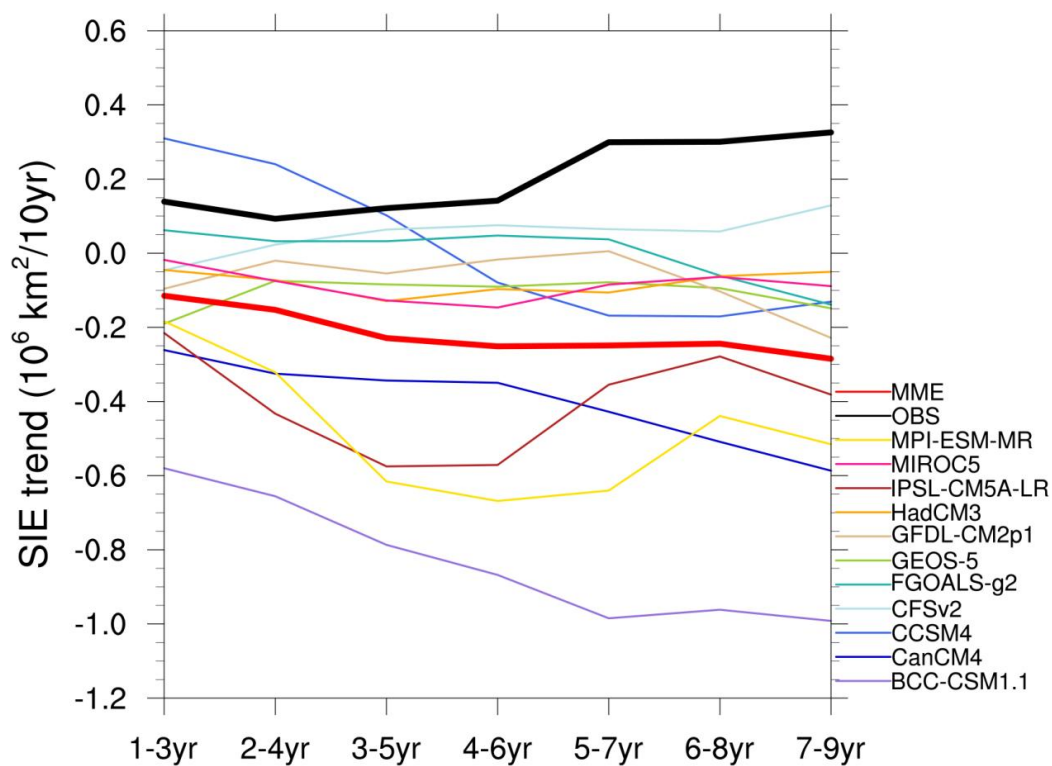
756
757
758
759
760
761

Figure 7. Time series of September Antarctic sea ice extent (seasonal minimum) from the simulations of the 10-year hindcast for each ensemble member of each individual model (thin gray line), the ensemble mean of each individual model (thick red line) and satellite observation (black line) from 1981 to 2015.



762
763
764
765
766
767

Figure 8. Anomaly correlation coefficients between the simulated and observed Antarctic September sea ice concentration anomalies for the lead-time of 1-year (top panel) and 3-5 years (bottom panel). The correlation coefficient 0.61, 0.73 and 0.88 represents 90%, 95% and 99% confidence levels, respectively.

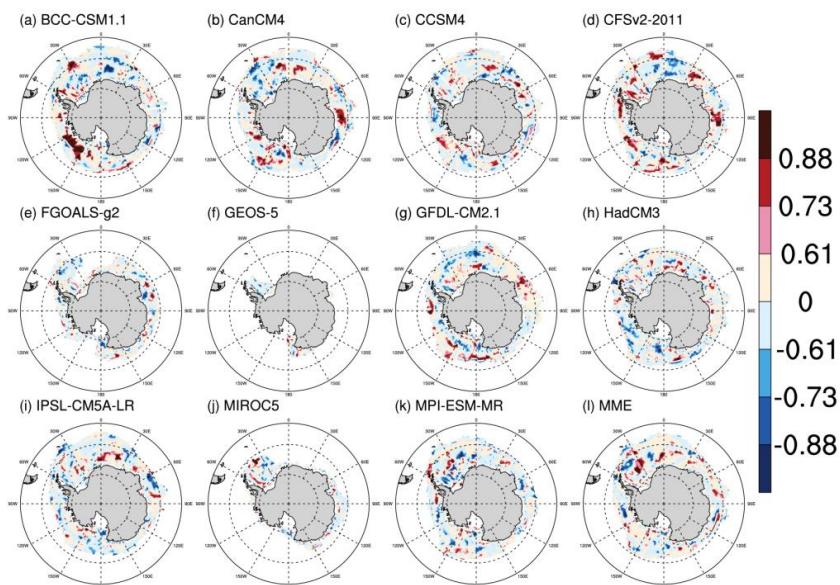


768
769
770
771
772

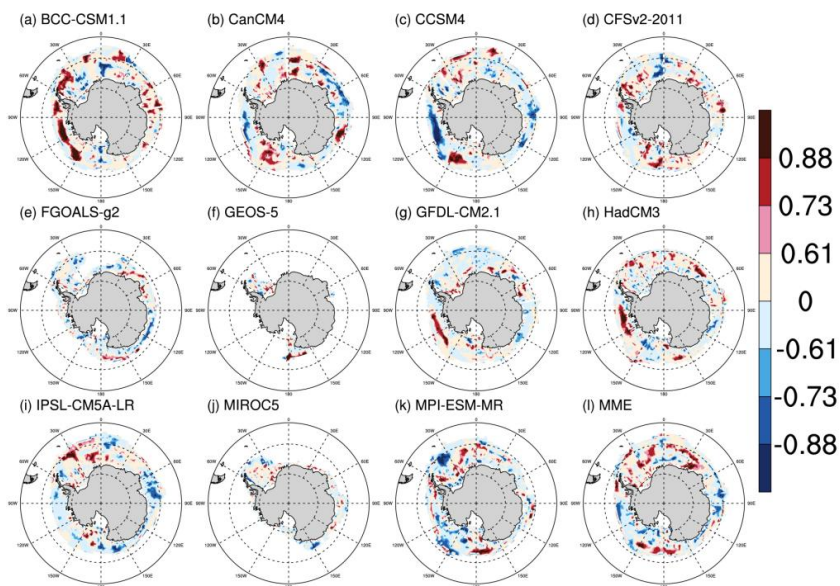
Figure 9. The predicted trends (slope of a linear regression) of September Antarctic sea ice extent anomalies as a function of the lead-time after applying a 3-year average.



1 Year

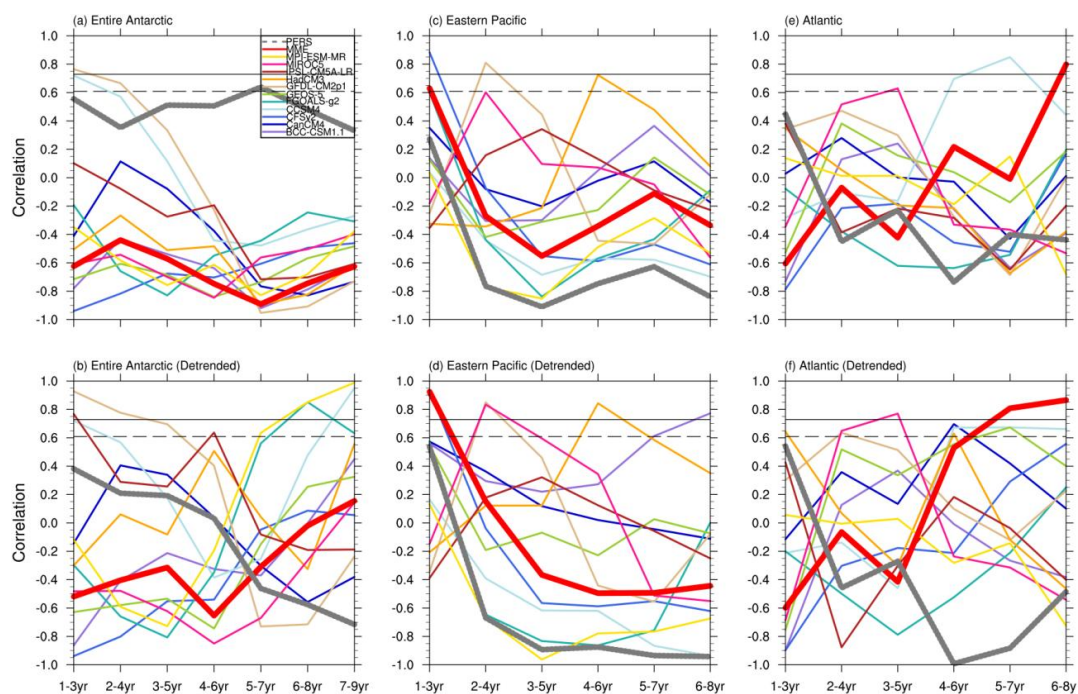


3-5 Year



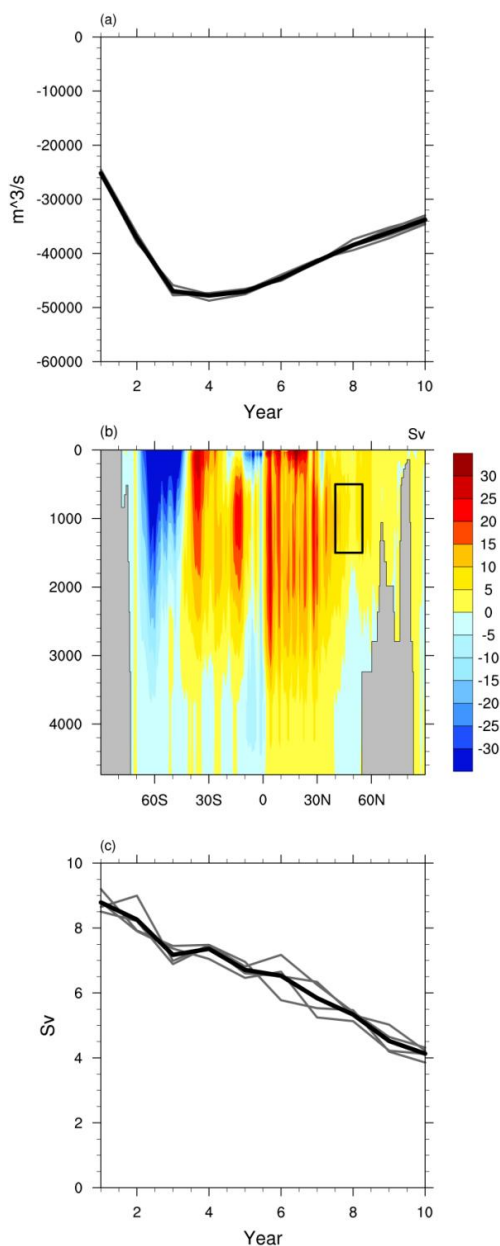
773
774
775
776

Figure 10. same as Figure 8, but for detrended September sea ice concentration anomalies.



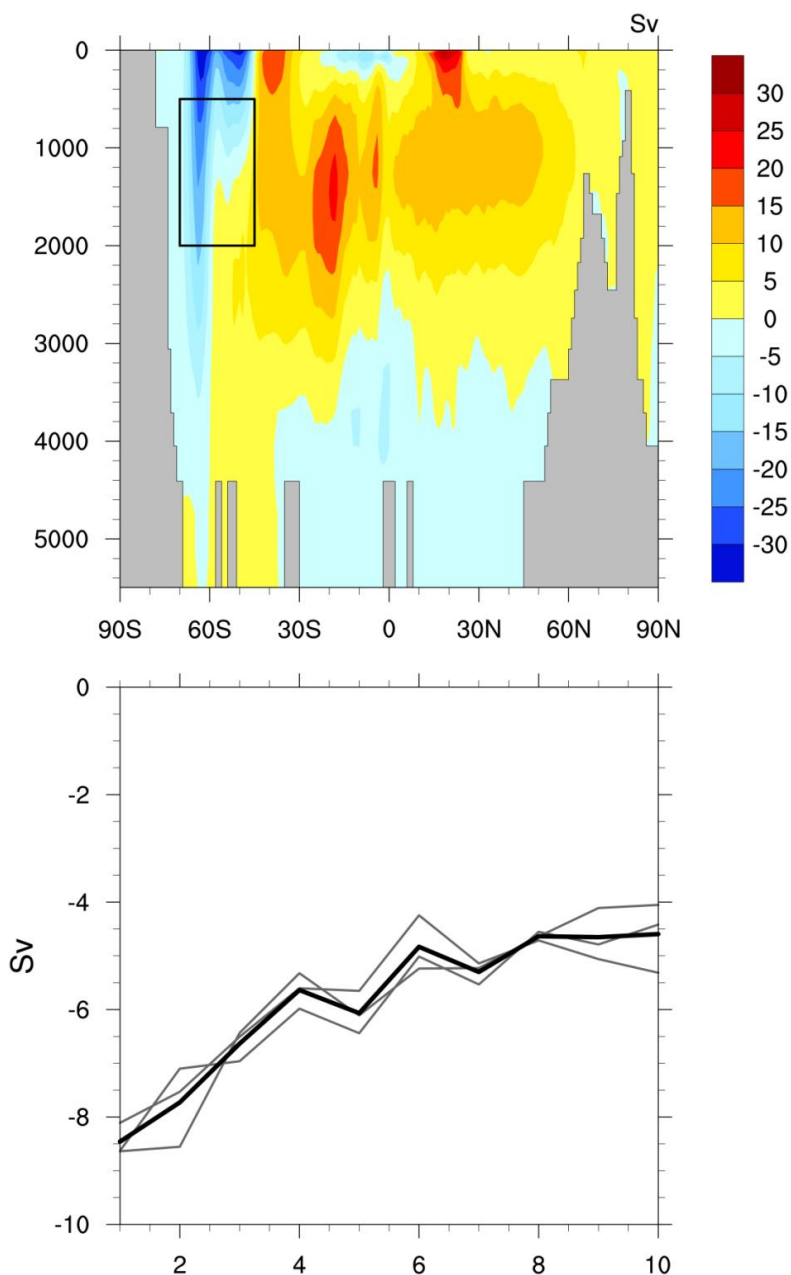
777
 778
 779
 780
 781
 782
 783
 784

Figure 11. Anomaly correlation coefficients between the simulated and observed Antarctic September sea ice extent anomalies for the three regional indices (the entire Antarctic, eastern Pacific and Atlantic) as a function of the lead-time. The top and bottom panels are the original and detrended time series, respectively. The horizontal dashed and solid lines represent 90%, 95% and 99% confidence levels, respectively. The thick gray line is the persistence prediction.



785
786

787 Figure 12. (a) Freshwater export through Fram Strait (the cross-section along 74°N and between
788 30°W and 10°E), (b) Atlantic Ocean meridional overturning streamfunction in September
789 averaged for all decadal hindcasts from 1981 to 2015 for the CFSv2 (upper panel) and (c) time
790 series of stream function averaged over 40-55N, 500-1500m as indicated by the black in upper
791 panel (lower panel). The thin gray line represents each ensemble member and the thick black line
792 represents the ensemble mean.



793
794
795
796
797
798
799
800

Figure 13. Atlantic Ocean meridional overturning streamfunction in September averaged for all decadal hindcasts from 1981 to 2015 for GEOS-5 (upper panel) and time series of streamfunction averaged over 45-70N, 500-2000m as indicated by the black in upper panel (lower panel). The thin gray line represents each ensemble member and the thick black line represents the ensemble mean.